國立交通大學

材料科學與工程研究所

博士論文

以電漿輔助式分子束磊晶成長應用於高電子遷移率電晶體之氮化鋁鎵/氮化鎵異質結構

Epitaxial Growth of AlGaN/GaN Heterostructure by Plasma-Assisted Molecular Beam Epitaxy for High Electron Mobility Transistor Applications

研究生：黃延儀

指導教授：張翼 教授

中華民國一百年七月

以電漿輔助式分子束磊晶成長應用於高電子遷移率電晶體之氮化鋁鎵/氮化鎵異質結構

Epitaxial Growth of AlGaN/GaN Heterostructure by Plasma-Assisted Molecular Beam Epitaxy for High Electron Mobility Transistor Applications

研究生：黃延儀　　Student：Yuen-Yee Wong

指導教授：張翼　　Advisor：Edward Yi Chang

國立交通大學

材料科學與工程研究所

博士論文

A Thesis Submitted to Department of Materials Science and Engineering
National Chiao Tung University
in partial Fulfillment of the Requirements
for the Degree of Doctor of Philosophy in
Materials Science and Engineering

July 2011

Hsinchu, Taiwan, Republic of China

中華民國一百年七月

以電漿輔助式分子束磊晶成長應用於高電子遷移率電晶體之氮化鋁鎵/氮化鎵異質結構

學生：黃延儀　　　　　　　　　　指導教授：張 翼 博士

國立交通大學材料科學與工程研究所

摘要

本論文利用電漿輔助式分子束磊晶在藍寶石基板上成長應用於高電子遷移率電晶體元件製作之氮化鋁鎵/氮化鎵異質結構。我們首先探討氮化鋁緩衝層成長條件對氮化鎵薄膜缺陷結構的影響。在較低溫度成長的氮化鋁緩衝層上，由於表面比較粗糙，氮化鎵薄膜裏的刃線差排密度會降低，但螺旋線差排密度會增加。這是因爲粗糙的氮化鋁表面有助於彎曲刃線差排的成長方向，促進刃差排的交互作並減低其密度。另一方面，粗糙的氮化鋁表面因爲有許多讓螺旋差排形成的成核點，導致螺旋差排的密度增加。進一步的試驗也發現刃線差排與氮化鋁緩衝層的厚度息息相關。大或小於最佳的厚度（15奈米)，都會造成氮化鎵薄膜的應力上升並增加刃線差排的密度。

爲了有效的降低差排密度，我們利用了在鎵貧乏成長條件下成長的氮化鎵緩衝層。鎵貧乏的氮化鎵緩衝層表面有許多小平臺及溝槽，溝槽裏的斜壁提供了很好的方法以彎曲刃差排的成長方向並促進差排得交互作用。通過提升差排的互相結合及消滅效應，鎵貧乏緩衝層能更有效的降低刃差排的密度。另，鎵貧乏緩衝層也能有效的抑制螺旋差排的產生。因此把鎵貧乏的氮化鎵緩衝層成長在平滑表面的氮化鋁緩衝層（可利用高溫成長）上，就能有效的減少氮化鎵薄膜裏的所有差排密度。爲了修復粗糙的氮化鎵緩衝層表面，我們也開發了氮化鎵的遷移促進磊晶技術。這方法是由交替沉積鎵和氮原子於試片表面上來完成。結合鎵貧乏的氮化鎵緩衝層及遷移促進磊晶技術，我們利用分子束磊晶成長出低差排密度（$\sim 2\text{x}10^{8}$ cm^{-2}）以及擁有平滑表面的氮化鎵薄膜。

最後，我們也研究了不同差排缺陷對氮化鋁鎵/氮化鎵異質結構的電性特性影響。

從霍爾量測中發現，其異質界面通道裏的二維電子遷移率主要受限於刃差排的密度。這是因爲刃差排缺陷趨向於捕捉電子，形成庫倫散射中心並減緩通道裏的電子遷移率和增加通道的阻值，所以刃差排將降低電子元件的電流密度和操作頻率。另一方面，從蕭基二極體的量測可得知，螺旋差排像有如讓縱向電流流通的路徑，非常不利於閘極的逆向偏壓漏電流，導致元件的崩潰電壓變差。因此，要製作高品質的高電子遷移率電晶體元件, 氮化鋁鎵/氮化鎵材料裏的各種差排密度必須降低。

Epitaxial Growth of AlGaN/GaN Heterostructure by Plasma-assisted Molecular Beam Epitaxy for High Electron Mobility Transistor Applications

Student: Yuen-Yee Wong　　　　　　Advisor: Dr. Edward Yi Chang

Department of Materials Science and Engineering

National Chiao Tung University

Abstract

AlGaN/GaN heterostructure for the high electron mobility transistor applications were grown by plasma-assisted molecular beam epitaxy (PA-MBE) on the sapphire substrates. The effects of AlN buffer growth parameters on the defect structure on GaN film were first investigated. For GaN film grown on lower-temperature buffer, the density of screw threading dislocation (TD) was increased while the density of edge TD was decreased. The rough AlN surface helped to bend the growth direction of edge TDs and then reduced the dislocation density through recombination and annihilation processes. However, the screw TD was increased on the rough AlN buffer because this surface provided many nucleation centers for screw dislocation. Further examinations revealed that the edge TD was also closely related to the AlN buffer thickness which corresponding to the stress in GaN film. Total TD density could be minimized by optimizing the AlN buffer growth temperature and thickness.

GaN buffer grown at Ga-lean condition was found useful to reduce the edge TD density in the GaN film significantly. The Ga-lean buffer, with inclined trench walls on its surface, provides an effectively way to bend the propagation direction and promotes the interaction of edge TDs in the GaN film. As a result, the edge TD density was reduced by approximately two orders of magnitude to $2x10^{8}$ cm^{-2}. The rough surface of Ga-lean buffer was recovered using migration enhanced epitaxy (MEE), a process of alternating deposition cycle of Ga atoms and N2 radicals, during the PA-MBE growth. By growing the Ga-lean GaN buffer on a

smooth AlN buffer (achieved by high temperature), both the edge and screw TDs in the GaN film could be effectively reduced.

Finally, the roles played by different types of TDs on the electrical properties of AlGaN/GaN heterostructure were studied. From the Hall measurement, the electron mobility in two-dimensional electron gas channel was mainly controlled by the edge TDs. The edge TD acted as Coulomb scattering centers inside the channel and reduced the carrier mobility and increased its resistance. On the other hand, from the Schottky barrier diode characterization, the screw TDs which acted at the current leakage path and was more deleterious to the gate reverse-bias leakage current of the AlGaN/GaN structure. As a result, the output current density and operating frequency of the HEMT devices were decreased by the edge TDs while the device breakdown voltage was degraded by the screw TDs. Therefore, for high performance HEMT device fabrication, both screw and edge TD densities in the AlGaN/GaN material have to be minimized.

1896

Acknowledgement

誌謝

2006 年初，有機會來到了張翼老師的實驗室(CSDLab)，展開了我在交通大學的博士生學習與研究生涯。幾年下來，非常感激張翼老師的教導以及所給于的各種機會。另外，實驗室及學校完善的半導體設備與交大材料所老師們提供的基礎教學訓練，讓我得以從頭學起半導體的相關材料與元件，真的受益非淺。

在來到交大的初期，很幸運的可以加入由楊宗熺學長領導的 MBE 長晶小組工作，讓我結交到一群非常要好的夥伴。除了宗熺學長還有哲榮，瑞泰，怡誠和詩國，我很懷念大夥兒一起學習，一起討論，一起去玩的日子，也感謝你們在日常生活上給于的各種協助，讓我在臺灣的生活倍感窩心。在利用 MBE 長晶的歲月裏，還要感謝 ULVAC 公司及員工,特別是陳江耀，陳建瑩，張晃崇學長等對機台的維修及保養所付出的努力，還有在試驗上的幫忙及支持。此外還要感激涂搏閔經常提供 GaN template 給我做實驗，多次的 Hall 量測及長晶方面的意見。

特別感謝 CSDLab 製程組的瑞乾，宗育，家達與昱盛在元件製作上的幫忙和電性量測上的協助。當然還有其他資深的學長如岳欽，建億，雲驥，你們的指導讓我對元件物理有了更深入的了解。還要謝謝龔梁，佑霖，偉進，Tung，Tinh 和電物所的振豪提供在長晶方面的協助。吳岳翰學長在 TEM 方面的專業協助也確實讓我增長了學多寶貴知識。

最重要的是要感謝我最摯愛的父母及家人，你們的包容與支持一直是我往前邁進的動力，也讓我有非常大的自由發展空間，可以盡情的做自己感興趣的事，過快樂滿足的人生。

在博士班的學習過程中曾經受過無數的恩惠，除了老師，學長，同學，朋友，還有學校的行政人員，認識或不認識的人士，也感謝你們。請原諒我沒能一一提及，除了感激，也祝福你們，願各位身體健康，萬事順利。

Contents

Chapter 1 Introduction

Chapter 2 Plasma-Assisted Molecular Beam Epitaxy System, Experimental Procedure and Characterization Methods

Chapter 3 Effect of AlN Buffer Growth Parameters on the Defect Structure of GaN Grown by Plasma-assisted Molecular Beam Epitaxy

Chapter 4 Dislocation Reduction in GaN film Using Ga-lean GaN buffer Layer and Migration Enhanced Epitaxy

Chapter 5 The Roles of Threading Dislocation on the Electrical Properties of AlGaN/GaN Heterostructure Grown by MBE

Table Captions

Figure Captions

Chapter 1

Introduction

1.1 Background

GaN is an interesting material because of its unique properties for both electrical and optical devices. With its wide direct bandgap and high electron mobility characteristics, GaN is an idea semiconductor material for the high power and high frequency electronics applications. Besides, GaN is also a physically hard material that makes it easier to handle during the fabrication. What has attracted earlier attention on this material is the fact that it can generate blue color light if made into the solid-state lighting devices, such as LEDs and laser diodes, completing the range of primary colors for lighting purposes. Despite the extraordinary properties of GaN material, to achieve device quality GaN is not easy. In contrast to the Si or GaAs materials, large-size native substrate for the growth of GaN materials is not available. This is the main obstacle which has hindered the progress of the GaN devices in the 1980s'. Fast development of GaN devices began following the successful attempt to grow high quality GaN crystal on sapphire for LED devices by Shuji Nakamura in the beginning of 90s' [1]. Apart from the optical devices, the remarkable properties of the GaN materials are also found its niche electronic applications. The high energy bandgap and high electron saturation velocity of GaN have made it the superior material for high-speed and high-power electronics applications, especially for the wireless communication equipment.

Table 1.1 describes some of the benefits of using GaN for electronic applications. In this thesis, the high quality GaN materials for the fabrication of electronic devices, especially the high electron mobility transistor, were grown using molecular beam epitaxy (MBE) on sapphire substrates.

1.2 AlGaN/GaN HEMTs

As described above, GaN high electron mobility transistors (HEMTs) are excellent candidates for high power and high frequency applications. GaN materials for HEMT fabrication consists of a higher bandgap material, such as AlGaN [2] or AlInN [3], growth on top of the GaN film as the barrier layer. The discontinuity in conduction bands between the two materials forms a 2-diamentional electron gas (2DEG) channel at the hetero-interface. The 2DEG enables better electron confinement and less carrier scattering. Therefore, high electron mobility (~2000 $cm^2/V\text{-}s$) can be achieved on an AlGaN/GaN heterostructure. AlGaN/GaN HEMT does not require intentional doping in the barrier or buffer layer to provide carrier in the 2DEG channel. Carriers in the 2DEG of GaN HEMT are originated from the material surface states and driven into the channel by the polarization field in the material (Fig. 1.1) [2]. Due to the strong polarization effect and large amount of surface states, high electron density (~1.5×10^{13} cm^{-2}) can be induced at the 2DEG by AlGaN barrier layer with Al~25%. As a result of both high mobility and high carrier density, AlGaN/GaN HEMT device of high current density (>2 A/mm) has been demonstrated [4].

1.3 Material growth of GaN

Due to the lack of large-size and low-cost commercial-grade native substrate, GaN materials are usually grown on the foreign substrates such as sapphire, silicon or silicon carbide. Table 1.2 shows some of the material properties of these substrates as compared to the GaN and AlN layers. Generally, the lattice constants and thermal expansion coefficients of these substrates differ significantly (except SiC) from that of GaN. As a result of these mismatches, large amount of dislocations are generated in the GaN film. The quality of the GaN film is therefore critically dependent on the ability of the transition layer (buffer layer) used to accommodate the stress generated from these mismatches. The commonly used buffer layers include low temperature GaN [1, 5], AlN [6-8] or their variations [9-11]. Dislocations generated in GaN are mainly screw, edge and mixed TDs. Besides the buffer layers, other approaches are also used occasionally to further improve the crystal quality of GaN film such as the insertion of AlN interlayers [12] or Si delta-doping layer [13] and the growth of GaN epilayers on a lateral epitaxial overgrown substrate [14] or a vicinal sapphire substrate [15].

High crystalline quality GaN materials are usually grown by metal-organic chemical vapor deposition (MOCVD) and molecular beam epitaxy (MBE) methods. MOCVD is famous for growing the LED-quality GaN and is also frequently used to grow GaN materials for HEMT applications lately. The main advantages of MOCVD, as compared to MBE, are the high growth rate and high crystal quality material even for the direct growth of GaN layers on the foreign substrates. Besides, MBE has also proven to be a promising technique to grow GaN materials for HEMT devices application [10, 12, 16]. The benefits of growing GaN with MBE include real-time monitoring of crystal growth with reflection high-energy electron deflection (RHEED), a carbon-free and hydrogen-free growth environment, a smooth surface, sharp interfaces and low point defect density. These attributes are important for achieving high quality materials for HEMT devices. Table 1.3 shows some important developments on the electrical properties of AlGaN/GaN structure grown by MOCVD and MBE techniques. Even though the measuring temperatures for the 2DEG mobility are varied for different works, the general tendencies are summarized as following:

(i) AlGaN/GaN structures grown on SiC has the best quality as compared to those grown on sapphire or Si substrates.

(ii) For direct growth of AlGaN/GaN structure on the substrate, MOCVD samples are better than MBE samples.

(iii) For AlGaN/GaN grown on the high quality GaN templates, the MBE samples are better than MOCVD samples.

The results indicate that the AlGaN/GaN structure grown on SiC has the best crystal quality due to the least lattice and thermal mismatches induced by the substrate. On the other hand, the difference for materials grown by MOCVD and MBE can be explained by the relatively poor ability of MBE to reduce the stress in GaN films when grown on the foreign substrates. For MOCVD growth, the transition from a three-dimensional low-temperature (525-600 ℃) GaN nucleation layer to a two-dimensional GaN growth on a sapphire substrate during the substrate temperate ramp-up to a higher process temperature (1060-1100 ℃) can effectively reduce the stress and improve the crystalline quality of a GaN film [17]. In contrast, the MBE growth process cannot achieve this transition due to the much lower growth temperature (700-800 ℃). Therefore, the MOCVD grown samples have a TD density up to 2 orders of magnitude lower than those grown by MBE. However, Table 1.3 shows that the best AlGaN/GaN structures were grown by MBE on the high quality templates. This indicates that the true ability of MBE may be revealed if the stress issue can be resolved. The following section will discuss the most important issues of GaN material grown by MBE technique on sapphire substrate.

1.4 Growth of GaN by MBE on sapphire

1.4.1 AlN buffer layer

For the growth of high quality GaN on sapphire substrate using MBE, an AlN buffer layer is indispensable. Other than acts as a transition layer, the AlN buffer also helps to achieve a Ga-face GaN grown by MBE [18, 19]. The Ga-face GaN has better crystal quality and smoother surface morphology as compared to the N-face GaN [20]. Furthermore, the Ga-face AlGaN/GaN structure also provides the proper polarity to produce an electrical field to induce carrier into the 2DEG channel for the HEMT device.

1.4.2 Growth temperature

The generally used growth temperatures of GaN materials by MBE fall in between 700-800 °C. While a lower growth temperature will degrade the crystal quality of GaN film, a growth temperature higher than this will enhance the desorption rate of Ga atoms from the substrate which will significantly reduce the growth rate and increase the Ga source consumption. However, as compared to the theoretically predicted melting temperature of GaN (~2500 °C), the MBE growth temperature is significantly lower than that normally required for other compound semiconductors (50~75% of material melting temperature) to achieve high quality single crystal film. The growth of GaN by MBE is therefore occurred under the thermodynamically meta-stable condition with a non-equilibrium kinetically-limited reaction [21].

1.4.3 III-V ratio

The III-V ratio is an important growth parameter for the GaN materials. It is referred as the ratio of active Ga and N atoms that available for the growth under a given substrate temperature. Hence, for an identical supply of Ga and N sources, the III-V ratio will change at different substrate temperatures. III-V ratio not only controls the crystal quality of MBE grown GaN but also significantly affect its surface morphology. The GaN surface morphology is determined by the following three growth conditions [22]:

(i) N-rich: rough surface with cratered morphology

(ii) Intermediate: large areas of uniform and flat surface but having pits and irregular, faceted edges,

(iii) Ga-rich: Smooth surface but with Ga droplets form on the surface.

Optimum growth condition, which is chosen somewhere in between the intermediate and Ga-rich regimes, will offer a smooth surface and without any Ga droplets

1.5 Objective of the study and organization of this thesis

In this study, the growth of high quality GaN material by MBE for the HEMT fabrication is investigated. All the materials were grown on the 2-inch c-plane (0001) sapphire substrate which is relatively cheap and available with high quality.

The thesis is divided into six chapters. The first chapter gives the background of the study. In the second chapter, detail descriptions on the MBE system, experimental procedures and the characterization methods are presented. Chapters 3 to 5 are the experimental results. The dependence of the defect structure of GaN film on the AlN buffer growth parameters was first investigated (Chapter 3). This understanding is important for improving the GaN crystal quality. With this understanding, an effective method by combining the Ga-lean GaN buffer and migration enhanced epitaxy was invented and the growth of high crystal quality GaN film by MBE using this approach will be described in Chapter 4. In Chapter 5, the roles of different dislocation types on the electrical properties of GaN HEMT grown by MBE are investigated. Chapter 6 concludes the study.

Table 1.1 Advantages of GaN material for electronic applications.

Material property	Advantages
Wide bandgap 3.42 eV	■ Great endurance for high device operating temperature ■ Suitable for high power applications. ■ Working under high temperature environment
High breakdown field ~5x10^6 V/cm	■ Larger power density
High thermal conductivity ~1.3W/cm K	■ Better heat dissipation, enhanced device performance ■ Easier device packaging
High saturate electron velocity ~2.7*10_7 cm/sec	■ Suitable for high frequency applications

Table 1.2 Material properties of GaN, AlN, Si, SiC and sapphire.

Material	a (Å)	c (Å)	Thermal conductivity (W/cm K)	Thermal expansion coefficient (In-plane, 10^{-6} K^{-1})	Lattice mismatch GaN/substrate (%)	Thermal mismatch GaN/substrate (%)
GaN	3.189	5.185	1.3	5.59	-	-
AlN	3.112	4.982	2.85	4.2	2.4	25
Si (111)	5.430	-	1.3	2.59	-16.9	54
6H-SiC			4.9	4.2	3.5	25
Sapphire	4.759	12.991	0.5	7.5	16	-34

Table 1.3 Comparison of 2DEG mobility and sheet carrier concentration of AlGaN/GaN structure grown by MOCVD and MBE on different substrates. MOCVD-GaN stands for GaN template grown by MOCVD; HVPE-GaN stands for GaN template grown by HVPE; Dislocation free-GaN stands for very high quality free-standing GaN template; the carrier mobility and concentration are measured at 300, 77, 4.2 or 0.3 K unless specify in the bracket; x is the Al content in AlGaN layer.

Growth Method	substrate	Al content x	2DEG mobility (cm^2/Vs) (Sheet carrier concentration (n_s (cm^{-2})))				Reference
			300K	77K	4.2K	0.3K	
MOCVD	SiC	0.2	2000 (1×10^{13})	9000 (8×10^{12})	11000 (7×10^{12})		Gaska *et al.*, (1999) [23]
	SiC	0.4	1990 (1.4×10^{13})				Higashiwaki *et al.*, (2008) [24]
	Sapphire	0.18				10300 (1.5K) (6.9×10^{12})	Wang *et al.*, (1999) [25]
	Sapphire	0.3	1300 (9.84×10^{12})				Liu *et al.*, (2006) [26]
	Sapphire	0.2	1700 (8.4×10^{12})				Tülek et al., (2009) [27]
	Silicon	0.26	1500 (8.2×10^{12})				Selvaraj et al., (2009) [28]
	Silicon		1800 (1×10^{13})				Arulkumaran et al., (2010) [29]
MBE	SiC	0.3	1500 (1×10^{13})				Corrion *el al.*, (2006) [16]
	Sapphire	0.19	1500 (9×10^{12})	10310 (6×10^{12})		12000	Li *et. el.*, (2000) [12]
	Sapphire	0.3	1310 (1×10^{13})				Manfra et al., (2002) [10]
	Silicon	0.25	1500 (7.9×10^{12})				Dumka et al., (2004) [30]
	MOCVD-GaN/ sapphire	0.09		24000 (2.5×10^{12})	60000 (4K) (2.25×10^{12})		Elsass *et. al.*, (2000) [31]
	MOCVD-GaN/ sapphire	0.28	2039 (1×10^{13})				Cordier *et al.*, (2007) [32]
	HVPE-GaN/ sapphire	0.06				80000 (1.75×10^{12})	Manfra *et. al.*, (2004) [33]
	Dislocation free-GaN/ sapphire	0.1	2500 (2.6×10^{12})			109000	Skierbiszewski *el al.*, (2005) [34]

(a)

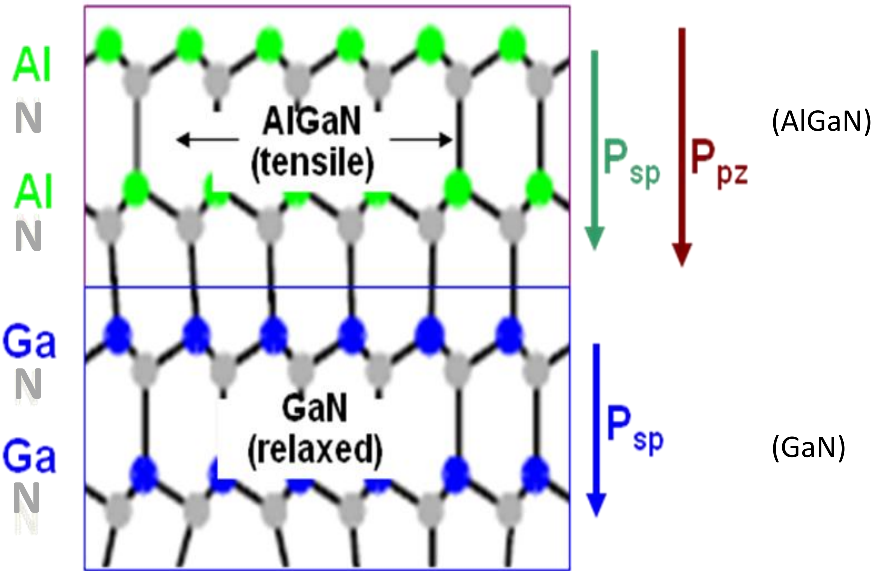

Net fixed polar charges at the AlGaN/GaN interface:

$P_{pz\,(AlGaN)} + P_{sp\,(AlGaN)} - P_{sp\,(GaN)}$

(b)

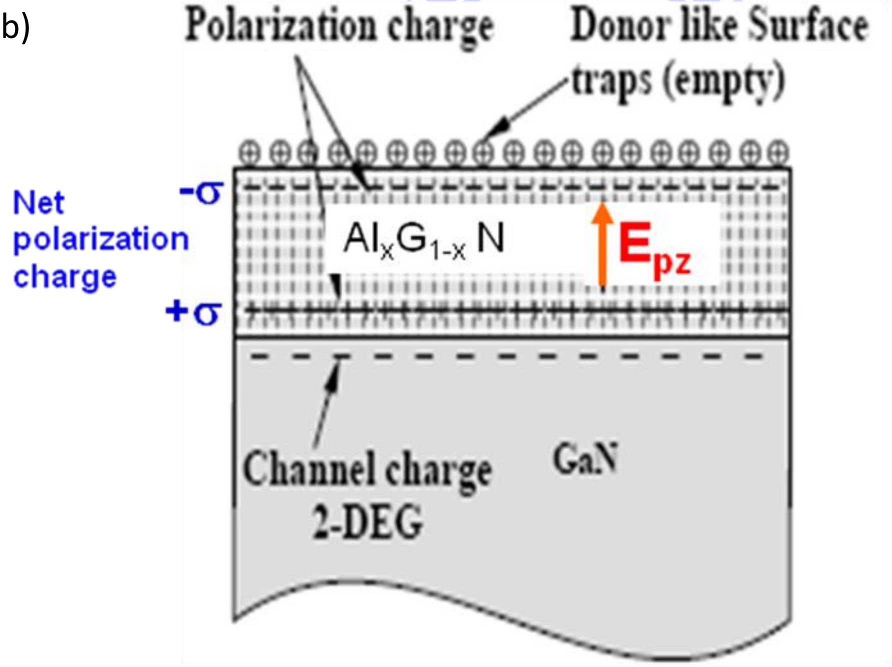

Fig. 1.1 (a) Polarization effect on the AlGaN/GaN structure. P_{sp} and P_{pz} are spontaneous and piezoelectric polarizations, respectively. **(b)** Carriers at the 2DEG are induced by the surface traps (charges) and polarization field in the AlGaN/GaN structure.

Chapter 2

Plasma-Assisted Molecular Beam Epitaxy System, Experimental Procedure and Characterization Methods

In this chapter, the plasma-assisted molecular beam epitaxy (PA-MBE) system used for GaN materials growth is introduced. The general procedure for the epitaxial growth will also be described. Finally, various measurement methods that used to characterize the material crystal quality and electrical performances of AlGaN/GaN devices are presented.

1896

2.1 Plasma-assisted MBE system

The PA-MBE system was designed by ULVAC Inc. for the epitaxy growth of group III-nitride materials. Both binary and ternary compound materials are grown using the group III sources of gallium (Ga), aluminum (Al) and indium (In) and group the group V source of nitrogen. The following sections describe briefly the important parts of the MBE system.

2.1.1 Chambers and vacuum pumps

The MBE system consisted of two chambers (Fig. 2.1): a sample preparation chamber or loading chamber (LC) and a growth chamber (GC) connected by a gate valve. A dry rotary pump (DRP) and a turbo molecular pump (TMP) are used in the LC. Pressure in the LC has to reach below $5\text{x}10^{-6}$ Pa before the sample is transferred into the GC. The GC, which is equipped with a rotary pump (RP), a TMP, a sputter ion pump and a titanium getter pump, has a base pressure <2x10^{-8} Pa. However, during the material growth, only the RP and TMP are used to maintain the growth pressure at the range of 5-8x10^{-3} Pa depending on the flow rate of the nitrogen gas.

2.1.2 Sample manipulator and growth sources

Sample holders (molybdenum) are available for 2, 4 and 6 inch substrates. The substrate surface is facing down when it is placed on a sample manipulator which is rotated by an external motor. Substrate rotation up to 10 rpm is applied to improve the deposition uniformity across the wafer. A substrate heater is located just above (behind) the sample holder to control the material growth temperature (up to about 850^{o}C). Four effusion cells are installed for high purity solid sources of Ga, Al (2 cells) and In. Source fluxes emerging from the effusion cell are controlled by the cell temperature (up to 1250^{o}C). Nitrogen source in the form of nitrogen radical is generated by two RF plasma generators. The amount of generated nitrogen radical is affected by the nitrogen gas flow rate as well as the RF power. Beside the plasma generator, nitrogen source from ammonia gas is also available by the installation of a hot-wired ‘cracking cell’. All the sources are deployed at the bottom part of the chamber and are co-focused onto the substrate holder (Fig. 2.1). A pneumatically controlled shutter is placed in front of each cell to control the sources used in material growth.

2.1.3 Analytical instruments and others

The ULVAC MBE system is equipped with a Reflection High Energy Electron Diffraction

(RHEED) for the real-time monitoring of epitaxial growth. High energy electron beam (20 keV), which is directed onto the sample surface at a grazing incidence (~2 degree), allows a surface-sensitive analysis during the growth.

An ionization gauge mounted at a flange on the chamber wall can be brought forward and place in front of the substrate to measure the source fluxes when necessary. In this way, the ionization gauge acts as a beam flux monitor (BFM) to calibrate the molecular beam intensity from time to time. A quadrupole Residual Gas Analyzer (RGA) is also placed at the rear part of the GC to detect the presence of the impurity gases in the chamber.

Both the growth chamber wall and source flanges are surrounded by liquid nitrogen (LN_2) cryopanels. LN_2 is flowed into the cryopanels during the growth process to prevent re-evaporation of impurities from parts other than the hot cells. The crypanels also provide thermal isolation among different cells.

2.2 Growth procedures

In this section, the general procedure for the growth of GaN material on sapphire substrate is described. The typical growth steps includes: sample preparation, nitridation, growth of buffer layer and growth of GaN epi-layer.

2.2.1 Sample preparation

The sapphire substrates used in this study were the commercial epi-ready 2-inch (50.8

mm) substrates with C-place orientation (<0001>). After loading into the growth chamber, the substrate was first annealed at ~820°C for about an hour to clean the surface. The cleanliness of substrate surface was monitored using RHEED. After the thermal treatment, a clear and sharp RHEED pattern appeared as shown in Fig. 2.2a.

2.2.2 Nitridation

After the thermal annealing, the sapphire surface was treated with nitrogen plasma in the so-called ‘nitridation’ process. During the nitridation, the sapphire surface (Al_2O_3) was converted slowly into a thin AlN layer. This layer acted as a starting layer for the epitaxial growth of AlN buffer layer. The effect of nitridation process on the crystal quality of GaN epilayer grown by the same MBE system was discussed in a previous study [35]. Without the nitridation process, the grown GaN material has low crystal quality and rough surface morphology. Furthermore, the nitridation temperature and duration are also important for the GaN epilayer growth. A rougher sapphire surface occurred after nitridation at high temperature (800°C) and it could generate more screw dislocations in the GaN film. On the other hand, nitridation performed at low temperature (200°C) would need longer time (90min) to transform the sapphire surface into AlN layer. In this study, substrate temperature of ~600°C and duration of 60min were chosen for the optimum nitridation result. The change of the surface structure of sapphire upon nitridation could be observed using RHEED. As shown in Fig. 2.2, the RHEED pattern of the original structure of Al_2O_3 (Fig. 2.2 (a)) changed to that of AlN structure (Fig. 2.2(c)) after one hour of nitridation.

2.2.3 Growth of buffer layer

Buffer materials generally used for the growth of GaN on sapphire substrate include low temperature GaN (LT-GaN), LT-AlN and high temperature (HT-AlN). In this study, AlN buffer layer was used. AlN not only improve the material quality of GaN but also help to achieve Ga-face GaN film grown by MBE on sapphire [18, 36]. Ga-face GaN provides polarization charges at the AlGaN/GaN interface for high electron mobility transistor (HEMT) fabrication. The effect of AlN growth parameter on the defect structure of GaN will be investigated in the Chapter 3. RHEED pattern on AlN grown on sapphire after the nitridation is shown in Fig. 2.3 (a).

2.2.4 Growth of GaN layer

The crystal quality of GaN film grown by MBE is determined by several factors such as the growth temperature, III/V ratio and the quality of buffer layer. The growth temperatures of GaN using MBE fall in a wide range from 650-800 °C [12, 16, 20, 34]. A higher growth temperature is preferable for better crystal quality but will enhance the desorption rate of Ga adatoms from the substrate. As a result, a larger Ga flux is needed to maintain a reasonable growth rate. On the other hand, the Ga/N ratio is used to control both the material quality and surface morphology of GaN. While a rough and low quality material is formed under the nitrogen rich growth condition, a smooth but with Ga metal droplets left on the GaN surface if too Ga-rich growth condition is used [20, 37]. Therefore, the optimum growth conditions for GaN with good quality and smooth surface (but without the Ga-droplet) can be achieved by the careful control of both the growth temperature and the Ga/N ratio. In this study, the growth parameters of GaN were initially optimized using a homoepitaxial growth approach. The homoepitaxial growth was carried out by depositing GaN film (~1μm) on a high-quality GaN film (~2μm) grown on sapphire by metal-organic chemical vapor deposition (MOCVD) (referred here as the GaN-template). This approach proved useful for achieving high-quality GaN film by MBE [33, 34]. Under the optimized growth condition, the crystal quality and surface morphology of GaN after regrowth should be identical with or better than that of the GaN-template. For the ULVAC MBE system, the growth parameters used are listed in Table 2.1. The growth rate of GaN is about 0.4 μm/hr under this growth condition. After that, the GaN material is grown directly on the sapphire by using an AlN buffer layer. In situ RHEED analysis during the GaN growth is shown in Fig. 2.3(b). The streaky RHEED pattern indicates that the GaN surface has a smooth surface morphology. After the growth was completed and the substrate was cooled down to below 200^{o}C, the RHEED pattern shows a 2x2 surface reconstruction (Fig. 2.3(c)) which indicates that the GaN has Ga-face polarity [38]. The effect of the growth conditions of AlN buffer layer on GaN quality will be discussed in Chapter 3.

2.3 Characterization measurements

In this section, the measurement methods used to characterize the material quality and electrical properties of GaN grown by ULVAC MBE system are described.

2.3.1 Field emission scanning electron microscope (FE-SEM)

The FE-SEM consists of a field emission electron source rather than a thermionic emission source used in a Thermal Tungsten wire SEM. A FE-SEM is therefore has a cold cathode. This SEM provides higher resolution imaging with higher beam density (brightness), and longer tip life. The primary electrons enter a specimen surface with energy of 0.5 to 30 keV to generate many low energy secondary electrons. The second electrons emission depends largely on the accelerating voltage of the primary electrons and also the probing incident angle on the specimen surface. In general, a large quantity of secondary electrons is generated from the protrusions and the circumferences of objects on the specimen surface, causing them to appear brighter then smooth portions. Under a constant accelerating voltage, an image of sample surface can thus be constructed by measuring the secondary electron intensity as a function of the position of scanning primary electron beam. In this study, Hitachi S-4700 FE-SEM is used routinely to check the GaN surface morphology as well as the film thickness.

2.3.2 Atomic force microscope (AFM)

AFM is used to check the surface topography of a material by measuring the interaction force between the AFM’s probe and surface structure. The AFM probe consists of a sensitive cantilever and a sharp tip (tip radius <10 nm) capable of obtaining the detail surface morphology of a material surface on the atomic scale if the scanning condition is carefully controlled. In general, the AFM is reliable to achieve lateral and vertical resolutions down to about 2 nm and 0.05 nm, respectively, in the ambient air environment. In this study, AFM Dimension 3100 system from Digital Instrument was employed to examine the surface information, such as morphology, roughness and density of pits, from the GaN material grown by MBE. This information provides the indications of the material quality and is a useful means to tune the growth condition.

2.3.3 High resolution X-ray diffraction (HRXRD)

HRXRD is the most powerful and commonly used characterization method to check the crystal quality of epitaxial grown materials. Besides being a non-destructive method, it also requires no sample preparation prior to the analysis. In this study, the Bede D1 HRXRD system (Fig. 2.4) equipped with a high power (2kW) X-ray source of Cu K_α line was used to determine the crystal quality of GaN grown by MBE. In additional to the crystal quality, other information of the GaN, such as lattice parameters, Al composition in the ternary compound of AlGaN and the AlGaN thickness were also determined by HRXRD. The following sections describe the frequently used scanning modes of the HRXRD in this study and its applications for epi-layer analysis.

2.3.3.1 Rocking curves (ω-scan)

Rocking curves were measured by scanning on the sample angle (or Omega) only. Such a scan is suitable for investigating the epi-layer crystal quality. In this study, it is assumed that the broadening of the rocking curve of a certain diffraction plane is mainly caused by the presence of threading dislocation (TD) in the GaN material. Three types of TDs are normally occurred in GaN: screw, edge and mixed TDs. These TDs can be distinguished by having different defect structures or Burgers vector, *b*. The *b* for screw, edge and mixed TDs are <0001>, 1/3 <11-20>), and 1/3 <11-23>, respectively. Due to this specific defect structure, the screw dislocation can distort all the ($h\ k\ i\ l$) planes with l non-zero, while the edge TD can distort only the ($h\ k\ i\ l$) plane with either h or k non-zero. Therefore, the GaN (0002) plane rocking curve is broadened by screw- and mixed-type TDs, while the GaN (10-12) plane rocking curve is broadened by all TDs [7, 39].

In order to estimate the TD density in the GaN grown by MBE, the rocking curves for both the symmetric plane (0002) and asymmetric plane (10-12) were scanned for each sample. Full-width at half-maximum (FWHM) of the rocking curves was determined by non-linear least-square fitting to a pseudo-Voight function. After that, an approach suggested by Gay *et al.* [40] as shown in equation (2.1) was used to estimate the TD density in GaN film:

$$D_{dis} \sim \beta^2 / 9b^2 \qquad (2.1)$$

where D_{dis} (unit = cm^{-2}) is the TD density in the material, β (in radian) is the FWHM of a given XRD peak, and b (Å) is the length of Burgers vector of their corresponding dislocation. For

GaN grown at the <0001> direction, the *b* of the screw TD is the GaN a-axis lattice constant, i.e. 3.189 Å while the b for the edge TD is the GaN c-axis lattice constant, while is equal to 5.186 Å. To simplify the calculation of dislocation density, the mixed TD was divided into screw- and edge-type TDs [7]. So the “screw TD’ used in this study was the sum of pure screw-type and the screw component of mixed-type TDs, while the ‘edge type’ was the sum of pure edge-type and edge component of the mixed-type TDs. In this way, the rocking curve width caused by the screw and edge TD in the GaN films can be estimated from the (10-12) rocking curve scan using the following equation:

$$\beta_{(10\text{-}12)}{}^{2}=\beta_{s}{}^{2}+\beta_{e}^{2} \qquad (2.2)$$

where $\beta_{(10\text{-}12)}$ is the FWHM of (10-12) plane, and β_s and β_e are the contributions of screw and edge TDs to the FWHM of (10-12) plane, respectively. Using equations (2.1) and (2.2), the screw and edge TD densities of GaN can be calculated. For example, if the GaN film grown by MBE showing the (0002) and (10-12) rocking curves of 100 and 1000 arcsec, respectively, then the estimated screw and edge TDs are $9.71\text{x}10^{6}$ and $2.54\text{x}10^{9}$ cm^{-2}, respectively.

2.3.3.2 Omega-2theta (ω-2θ) scan

ω-2θ scan was performed by scanning the sample and detector angles together in a 1:2 ratio. Such a scan is usually used to check the sample which contains thin and lattice mismatched layers. Diffraction signals from layers with different lattice constants along the diffraction plane will appear at different scanning angles. ω-2θ scan is therefore useful to compare the relative change in lattice constant due to residual stress or composition variation. In this study, ω-2θ scan was normally used to determine the Al composition in the AlGaN layer grown on GaN layer. Thickness of AlGaN can also be calculated from the simulation and data fitting from the ω-2θ scan.

2.3.3.3 X-ray reflectivity (XRR) scan

XRR is performed at a grazing incidence beam is suitable for studying surface and layers near the sample surface. By fitting the scanned patterns, layer information such as film thickness, surface and interface roughness can be obtained. This is especially useful for the top layers with thickness less than a few hundreds of nm and roughness less than 35 Å (root-mean-square). Even though the thin layer can either be single crystal, polycrystalline or amorphous material, XRR is always used in this study to determine the thickness of the thin AlGaN or AlN/AlGaN layers (<30 nm) which grown on top of the GaN film.

2.3.3.4 Reciprocal space mapping (RSM)

RSM is used to distinguish the strain and tilt in a sample. A series of scans of ω-2θ at different ω offset angles is performed and then converted into a map of diffraction intensity in the reciprocal space. RSM can be performed on both symmetric and asymmetric planes. When a RSM is performed on the symmetric planes of the substrate and an epilayer, the tilt angle of the epilayer with respect to the substrate can be observed. Besides, the relative out-of-plane lattice parameter of these two materials can also be calculated. Meanwhile, when a RSM of the asymmetric planes is obtained, both the relative in-plane and out-of-plane lattice parameter of the substrate and epilayer can be calculated. In this study, the RSM of asymmetric plane (such as (10-15) plane) was scanned occasionally to determine the strain and the Al composition of the thin AlGaN layer grown on the GaN film.

2.3.3.5 Triple axis diffraction

The few HRXRD modes described above are performed under the double axis configuration, i.e. without an analyzer crystal being installed at the detector stage. On the other hand, if an analyzer crystal is used as in the triple axis configuration, the acceptance angle of the detector was reduced to a few arcsec, allowing a finer definition of the scattering angle, 2θ. With such a high accuracy, the deflection angle from a certain crystal plane can be used to calculate the lattice constant of the scanned material. In this study, the triple axis configuration was used to determine the c-axis lattice constant of the GaN by obtaining the 2θ value of the (0002) plane.

2.3.4 Transmission electron microscope (TEM)

TEM is the powerful tool to characterize the epitaxial layer microstructure. Operating on the basic principles of the optical microscope, the TEM takes the advantage by using electron beam source which has much shorter wavelength as compared to the optical source. Therefore, the resolution of TEM can reach to about 0.2 nm, in the ideal imaging condition, in contrast to an optical microscope which can only reach to 200 nm. Besides the imaging capability, the

TEM is also equipped with other analytical tools such as energy dispersive spectroscopy (EDS) and electron energy loss spectroscopy (EELS) for material chemical composition analysis. In this study, the JOEL 2010F TEM system operated at 200 kV was used occasionally to check the crystal quality and microstructure of the GaN grown by MBE. Besides, the TEM was also employed to study the dislocation bending behavior in the GaN as a function of the buffer layer growth parameters. For sample preparation, the GaN/sapphire materials for TEM analysis were prepared either by focused ion beam (FIB) or conventional mechanical polishing and followed by an Ar-ion milling process.

Since the GaN materials grown in this study were meant for the fabrication of high electron mobility transistor (HEMT), the electrical properties of the grown materials therefore needed to be characterized. Some important characterization methods include the Hall effect measurement, the capacitance-voltage, current-voltage and direct electrical current measurements are briefly described below. All the samples for Hall measurement and for both the SBD and HEMT devices were fabricated using in-house facilities.

2.3.5 Hall effect measurement

The Hall effect measurement is an important characterization method for the semiconductor materials in determining the electrical resistivity, carrier density, carrier types and the mobility. In this study, the grown material structure for HEMT fabrication consisted of a thin AlGaN layer on the GaN film. Such a structure generates a 2-dimensional electron gas (2DEG) at the interface, which plays the most important role in the HEMT devices. The electrical properties, such as sheet resistivity, sheet electron density and electron mobility of the 2DEG were regularly determined by the Hall effect measurement system (Bio-rad HL55Win). The measurements were conducted in a Van der Pauw (VDP) configuration at room temperature.

2.3.6 Capacitance-voltage (CV) and current-voltage (IV) measurement

Schottky barrier diodes (SBD) with a circular Schottky contact surrounded by an ohmic ring were prepared for the CV and IV measurements. The CV measurements can be used to determine the charge concentration in the AlGaN/GaN structure as a function of depth from the material surface (estimated from the applied depletion voltage). Therefore, it is useful to check the carrier density in the 2DEG channel or the presence of carrier in the buffer layer of the AlGaN/GaN structure. On the other hand, the IV measurement on the SBD can be performed by applying the Schottky contact with different biases, from positive to negative as relative to ohmic contact. The measured current from the Schottky contact during the negative bias is of particular interest because this implies the leakage current through the AlGaN barrier layer. In this study, the CV and IV on the SBD were measured using an HP4284A LCR meter and a Kethley 4200 semiconductor analyzer system, respectively.

2.3.7 Direct electrical current (DC) measurement

After the fabrication of HEMT device on the AlGaN/GaN structure, DC measurements were carried out using an Agilent E5270 system. These include the measuring of drain currents at different drain voltage (I_d-V_d), the transconductance ($G_m=dI_d/dV_g$) and the threshold voltage (V_{th}). The I_d-V_d values depend on the carrier concentration and mobility of the 2DEG while G_m reflects the gate modulation ability and higher value is required for high frequency applications. Another important parameter for the HEMT devices is the off-state breakdown (BV_{off}). BV_{off} is determined by the breakdown voltage (defined as $I_d > 1$ mA/mm) measured by fully depletion of the channel (2DEG in the case for AlGaN/GaN) charges. High value of BV_{off} is required for high power HEMT operations.

Table 2.1 The optimized growth parameters of GaN using ULVAC MBE system.

Growth temperature	Nitrogen plasma	Ga flux
(^{o}C)	(RF power, N_2 flow rate)	(partial pressure, Pa)
740	GUN1: 450W, 4.0sccm	$4.8\text{x}10^{-5}$
	GUN2: 450W, 1.5sccm	

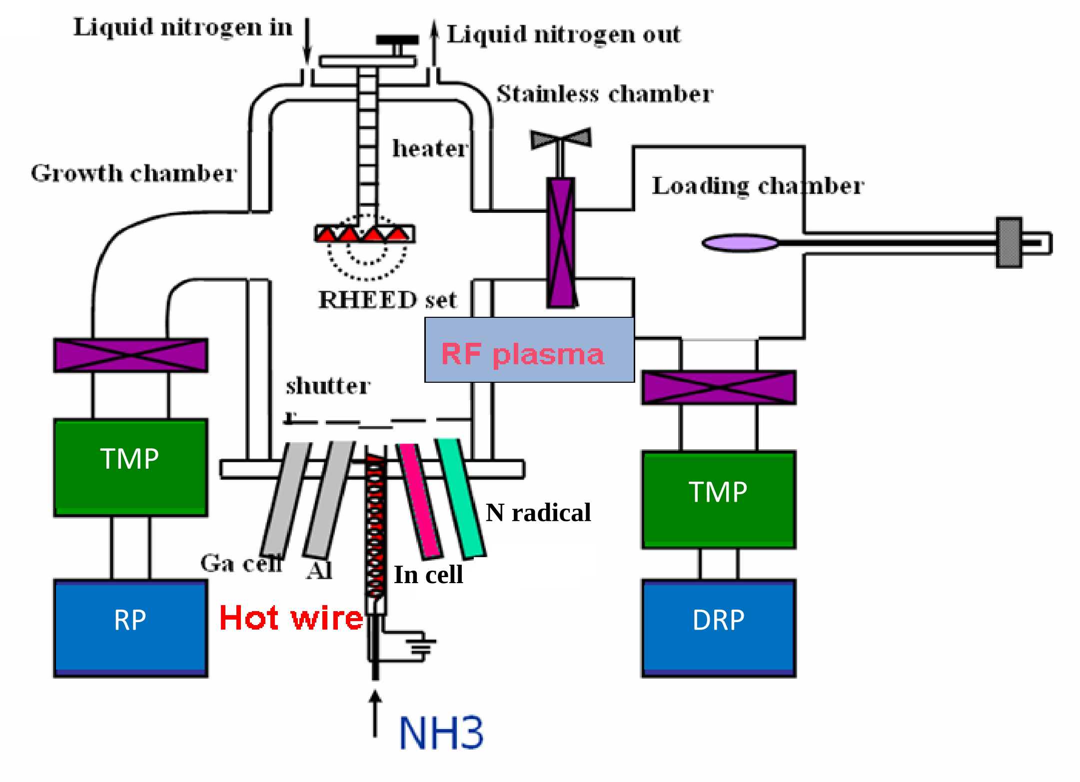

Fig. 2.1 Schematic diagram of the PA-MBE system.

1896

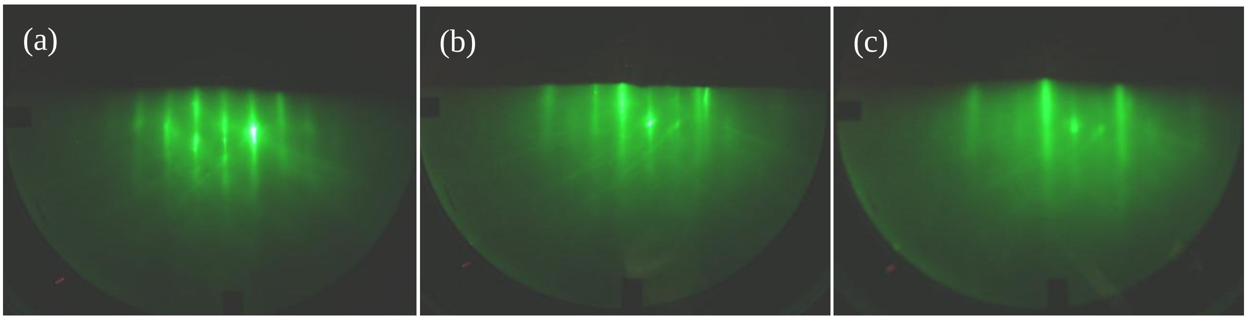

Fig. 2.2 RHEED pattern of sapphire substrate (a) before nitridation, (b) after 30min nitridation and (c) after 60min nitridation.

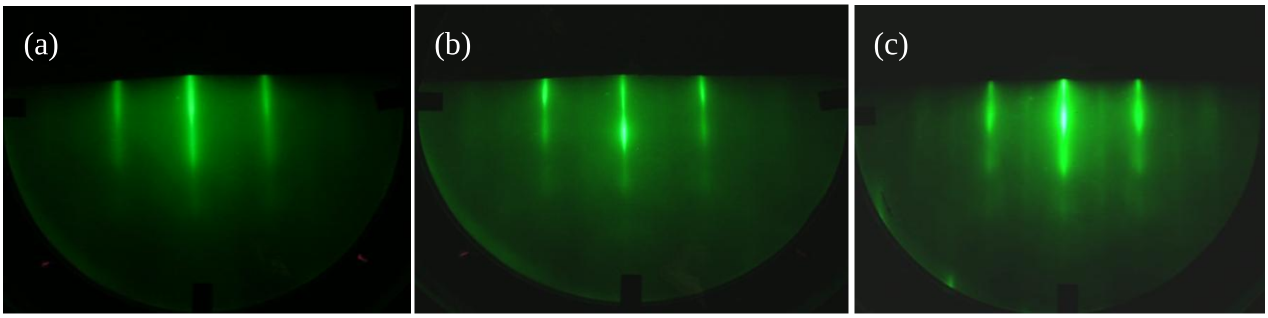

Fig 2.3 RHEED pattern of the surface of (a) AlN, (b) GaN during growth and (c) GaN after cooling to <200°C.

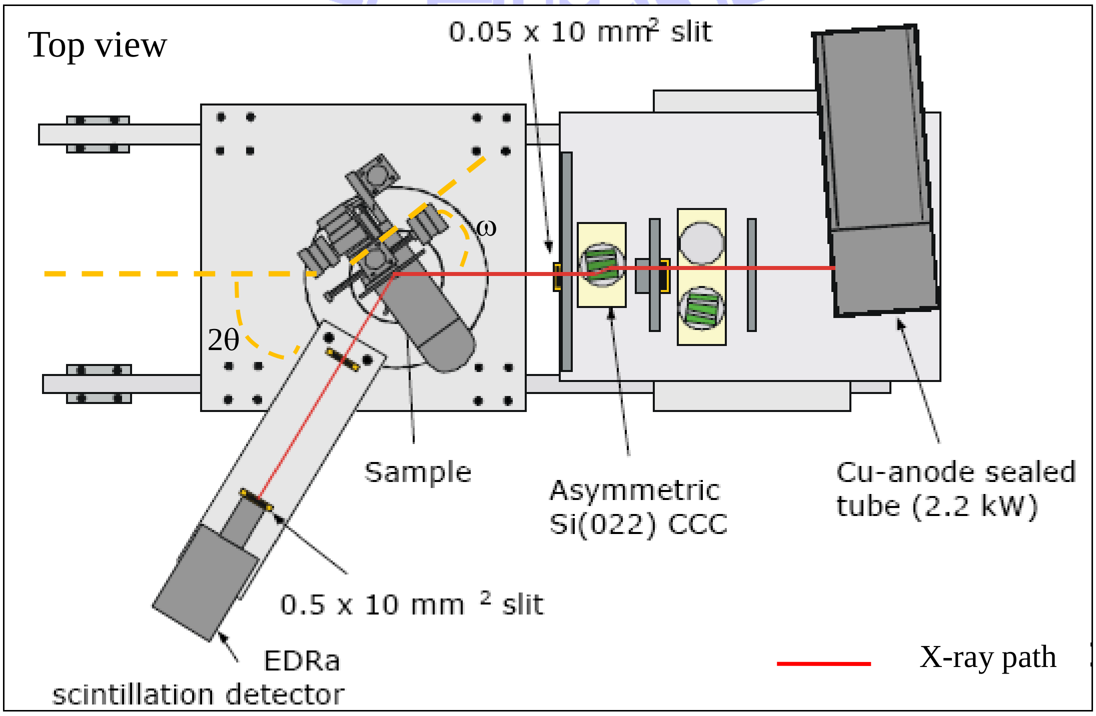

Fig. 2.4. Schematic diagram of the BEDE D1 HRXRD system.

Chapter 3

The Effect of AlN Buffer Growth Parameters on the Defect Structure of GaN Grown by Plasma-Assisted Molecular Beam Epitaxy

3.1 Introduction

For GaN grown on sapphire substrate using MBE, an AlN is necessary to achieve a high crystal quality Ga-face GaN. The Ga-face GaN is also required to provide the proper polarity to induce carrier into the two-dimensional electron gas (2DEG) at the AlGaN/GaN interface for HEMT device fabrication. Despite the use of AlN buffer, GaN grown on sapphire is still associated with high dislocation density (~10^{10} cm^{-2}). Intensive studies and various approaches have been carried out to reduce the dislocation density in GaN, however, little is known about the relationship between the different kinds of defect structures. In this chapter, the dependence of different kinds of dislocations on the growth parameters of AlN buffer is investigated. The understanding of their relationship can be used to reduce the total dislocation density in GaN.

3.2 Experiment procedures

Prior to the growth of AlN buffer layer and GaN films, standard high temperature annealing and nitridation processes were carried out as described in Chapter 2. AlN buffer layers of different growth temperatures (from 450 to 840 ^{o}C) and thicknesses (from 4 to 30nm) were prepared for the deposition of a 2-μm GaN film grown with constant growth parameters. In the first part of these experiments, AlN with constant thickness of 15 nm was used. Six samples (labeled as A-F) were prepared as shown in Table 3.1. In situ RHEED was used to monitor the growth of the AlN and GaN films. RHEED patterns on all the GaN films grown in our experiment were streaky indicating a flat surface (will be determined later) during growth and showing 2x2 surface reconstruction upon cooling (indicating a Ga-face polarity [38]) as shown in Fig. 3.1. On the other hand, the RHEED pattern for AlN was somewhat less streaky indicating that their surfaces were less smooth as a result of lower than unity Al/N ratio was used [41]. This ratio was chosen to avoid the formation of Al droplets on the AlN and cubic face GaN at the hetero-interface which could deteriorate the GaN quality [6, 41].

3.3 Results and discussion

3.3.1 Influence of growth temperature

Defect structures of the GaN films were determined by high resolution x-ray diffraction (HRXRD). Using double-axis configuration, the rocking curves (ω-scans) for both the symmetric plane (0002) and asymmetric plane (10-12) were scanned for each sample. Full width at half-maximum (FWHM) of the rocking curves was determined by non-linear least-squares fitting to a pseudo-Voight function. Table 3.1 summaries the rocking curve widths of GaN (0002) and (10-12) planes grown on different growth temperature AlN buffers.

As shown, the (10-12) FWHM was reduced with the increase of (0002) FWHM. Or in other word, the reduction of the total dislocation density in GaN film was associated with an increase of screw or mixed TDs when lower temperature AlN buffers were used.

The dislocation densities in GaN film were estimated from the HRXRD method as described in Section 2.3.3.1. Both the screw and edge TD densities of GaN were calculated and the results are plotted in Fig. 3.2. This figure clearly shows that the edge TD density in GaN film was reduced with the increase of screw TD density. In general, GaN film grown on lower temperature buffer have a lower edge TD density and higher screw TD density than GaN films grown on higher temperatures buffer. Even though the edge TD is dominated in all cases, consistent with previous studies of MBE-grown GaN [6] [39], it can be effectively suppressed with the use of a buffer layer grown at lower temperature. The edge TD density reduced from $1.5\text{x}10^{10}$ to $3.3\text{x}10^{9}$ cm^{-2} when temperature was decreased from 840 to 450 ^{o}C. Since the edge TD densities were at least an order of magnitude larger than that of the screw TD (except sample F), the total TD density was also reduced at the similar trend (from $1.5\text{x}10^{10}$ to $3.9\text{x}10^{9}$ cm^{-2}) despite a significant increase of the screw TD density in the film. On the other hand, the generation of screw TD was restricted by using higher temperature buffer layers. Screw TD density as low as $4.1\text{x}10^{6}$ cm^{-2} was achieved for GaN film grown on the 840 ^{o}C AlN buffer.

3.3.1.1 Correlation between defect structure and residual stress

Further study was carried out to investigate the correlation between defect structure in GaN films and growth temperature of AlN buffer. It is well known that the residual stress can cause the formation of dislocation in a material. Thus the stress in GaN is also believed to have played a role to manipulate the defect structure in it. The stress in our GaN film was determined by measuring the strain in the GaN lattice constants. Because the GaN epilayer grown on sapphire exhibits in-plane isotropic elastic properties, its in-plane stress (σ) can be described by the lattice strain (ε) from the relationship: $\sigma = M\varepsilon$, where M is the biaxial elastic modulus of GaN. In order to accurately calculate the stress in GaN film grown on sapphire, however, more comprehensive XRD surveys on various asymmetric planes are needed [42]. In this study, the stress states in GaN films were represented by the deformation of its c-axis lattice constants (ε_c). When the hexagonal GaN film is biaxially stressed on sapphire, its in-plane lattice deformation (ε_a) is associated with out-of-plane lattice change as described by the relationship: $\varepsilon_c \propto -\varepsilon_a$. Thus, the stress states in the GaN can be illustrated from the deformation of its c-axis lattice constant. Using triple-axis configuration from the same x-ray diffractometer (as described in Section 2.3.3.5), the deflection angles of (0002) plane were obtained with high accuracy (within a few arcsec) to determine the c-axis lattice constant of GaN films grown on different temperature AlN buffers. Fig. 3.3 shows that the edge TD density was increased proportionally with the strain in the GaN film. All the films were compressively stressed with their c-axis lattice constants elongated to different degrees.

Increment of the edge TD density from 3.3x10^9 to 1.5x10^{10} cm^{-2} corresponded to the elongation of the c-axis lattice constant from 0.15 to 0.38 %. Therefore, the result reveals that the stress in the GaN film has a significant influence on the edge TD as well as the total defect density. For comparison, the data for GaN film grown on the Ga-template (total thickness of about 1 μm) is also shown in Fig. 3.1. The edge TD density of this sample was only 2.5x10^8 cm^{-2}, with the c-axis lattice constant elongated to merely 0.09 %. This means that the GaN grown on the GaN-template has the least inherent stress and, thus, the best crystal quality.

From the result shown in Fig. 3.2, it appeared that the screw and edge TD densities were controlled by the properties of AlN buffers. To clarify this, we have carried out another set of experiment to grow only the AlN buffer layers on sapphire without GaN films on them. The growth procedure was identical to that described before. After the AlN buffers with nominal thickness of 15nm were deposited at temperatures shown in Table 3.1, substrate temperatures were briefly increased/ decreased to the growth temperature of GaN before it were cooled to room temperature. The crystal property and the surface morphology of these AlN buffers were characterized using XRD and AFM, respectively. Here, due to weak signals from the thin AlN layers, only rocking curve of its symmetrical (0002) plane was scanned. It was surprisingly to find out that the width of (0002) rocking curves of all the samples were almost the same, varied between 119 and 128 arcsec, without a clear changing trend against their growth temperature. The small variation in rocking curve widths has suggested that the crystal quality of AlN was not affected by the different growth temperatures used in this study. However, results from the AFM scans have shown that the surface roughness of AlN layers was decreased gradually when the growth temperature was increased in the experiment. In Fig. 3.4, three representative AFM images show that the surface roughness (rms) of AlN grown at 450, 740 and 840 ^{o}C were 0.42, 0.29 and 0.19 nm, respectively. For AlN grown at lower temperature, the shorter diffusion length of Al atoms was seemed to create more nucleation sites on sapphire when they were reacted with the nitrogen radicals. The AFM images also show that the density of these “nuclei” was larger on a lower temperature AlN surface. These results, thus, imply that the distribution of different defect structures in the GaN was influenced by the surface roughness of AlN buffer layer. Higher screw TD density was generated in the GaN film when grown on the rougher AlN buffer surface. This is agreed with the finding of Shen *et al*. [43], which has suggested that the small nuclei on AlN buffer were the origin of spirally growth features that further developed into screw TD in the GaN film. On the other hand, the edge TD density was reduced with the AlN surface roughness. This phenomenon will be discussed later.

In view of the different roughness in AlN buffers deposited at different temperatures, we have also investigated the surface morphology of GaN films grown on them. SEM images (Fig. 3.5) show that the surfaces of GaN films were flat for samples C to F (with AlN buffer temperatures increased from 525-840 ^{o}C, only image of sample C was shown in Fig. 3.5 (a)).

The surface roughness (rms) of sample C (roughest among the samples C to F) was 0.56 nm on a 1x1 um^2 area. However, for GaN films grown on AlN buffers lower than 525 ^{o}C, some hexagonal shape features were appeared on the GaN surfaces as shown in Fig 3.5 (b) and (c) for sample B and A, respectively. These features could most probably be related to the screw or mixed types TDs which are always grown following a spiral course into a surface hillock with hexagonal boundary [20, 44]. Some of these features were quite large (3-4 microns) and with hexagonal-like polygon boundaries, especially for those on sample A. This might caused by the clustering of many screw/mixed TDs grown in the close vicinity. Therefore, it is believed that these features were the consequences of rough AlN surface grown below 525 ^{o}C and high screw/mixed TD (>10^8 cm^{-2}) in the GaN film.

3.3.2 Influence of AlN thickness

In this study, it is particularly interested at the formation origin of edge TD, which is dominant in GaN grown by MBE and more deleterious to the material electrical properties. As seen before, the edge TD was closely related to the stress in GaN film which controlled by the growth temperature of AlN. Now, we would also like to see the effect of AlN thickness on the edge TD in GaN films. AlN grown at 525 ^{o}C with relatively lower edge TD density and smooth surface has been chosen to further investigate the influence of buffer thickness on the edge TD density. GaN grown on AlN deposited at 525 ^{o}C but with different thicknesses (from 4-30nm) were prepared. The changes of both GaN edge TD density and lattice strain on AlN thickness were illustrated in Fig. 5.6. As shown, the lowest strain and lowest edge TD density were achieved on a 15-nm thick AlN buffer. This value is comparable to those reported by other groups (~20 nm) for optimized GaN quality [10, 12]. Besides, the screw TD densities were about the same for all these samples (~6x10^7 cm^{-2}, not shown here). For GaN grown on sapphire by MBE, AlN is always used to achieve Ga-face GaN. Although AlN has a lattice constant intermediate between film and substrate, it is physically harder and thermally more stable than the GaN buffer which is normally used in metal-organic chemical vapor deposition (MOCVD). The stress in the GaN film is therefore more difficult to relax when an AlN buffer is used. A survey done by Pankove *et al*. [45] has shown that GaN grown on AlN buffer experienced larger stress than GaN grown on a GaN buffer. Therefore, a MBE grown sample is always associated with larger stress than those grown using MOCVD. It is thus logical that larger AlN thickness will induce larger stress values in the GaN [46]. Unexpectedly, however, larger stress is also encountered in GaN film grown on AlN thinner than 15nm (Fig. 5.6). More studies should be conducted to understand the stress-relaxation mechanisms caused by AlN buffer layer.

From all the above findings, we would now wish to discuss the effect of AlN growth parameters on the formation of edge TD and residual stress in GaN. For GaN grown on sapphire, the large stress generated should be relieved through the formation of misfit dislocation (at the materials interface) and/or plastic deformation in the crystal (achieved with dislocation glide). However, because the dislocations mobility in GaN is very much lower than other III-V materials [47], the probability for them to glide in the crystal was low. Therefore, the edge TD density and its distribution were frozen in the GaN epilayer after growth and the lattice strain could not be relaxed through the plastic deformation [48]. In this case, the amount of edge TD could be used to trace the stress state in the GaN film (Fig. 3.3). Furthermore, since all the GaN films were grown at the same temperature, the amount of stress generated from thermal expansion difference was the same for all samples. So, the difference in residual stress of our GaN films should be a result of AlN surface roughness. The surface roughness of buffer layer might have induced the inclination of TDs in GaN [49], started from the AlN/GaN interface. The inclined TDs could promote the interaction of edge TDs, along the growth direction, and provided a misfit dislocation component that relieved the stress in GaN [49, 50]. At the same time, the interaction of edge TDs with Burgers vectors of different signs could also enhance the recombination and annihilation of TDs [50, 51]. Therefore, the reduction of stress and edge TD density in GaN were achieved with the formation of inclined TDs. On the other hand, however, for screw TDs, which all have Burgurs vectors with similar signs, recombination and annihilation of TD could not occur though interaction. Thus, the screw TD could only cluster together but their amount was not reduced as what we have seen.

3.4 Conclusions

The effects of AlN buffer growth temperatures and thickness on the defect structure of GaN film were investigated. The buffer growth temperature controlled but has contrary effects on the screw and edge TDs densities. When grown on a lower temperature AlN buffer with rougher surface, the edge and total TD densities in GaN were effectively reduced. This phenomenon can be explained by the formation of inclined TD that promoted the reduction of both stress and edge TD in GaN. Beside, this stress was also affected by the buffer thickness. For the AlN buffer thinner or thicker than the optimum value, more stress and higher edge TD density were generated in GaN film. Thus, the edge TD density can be used as an indication of the stress state in GaN. On the other hand, the screw TD was increased with the used of lower temperature AlN buffer (with rougher surface) but not affected by the buffer thickness. In this study, GaN film grown on a 15nm thick buffer grown at 525 ^{o}C has a smooth surface (rms=0.56 nm) and relatively low total TD density ($5.8x10^{9}$ cm^{-2}). Smooth surface with low TD density are the two important factors for high performance electronic device fabrication.

Tables 3.1 FWHM of GaN (0002) and (10-12) planes grown on different AlN buffer growth temperatures.

Sample	A	B	C	D	E	**F**
AlN buffer growth temperature (^{o}C)	450	485	525	740	800	840
FWHM of (0002) plane (arcsec)	797	636	252	180	79	65
FWHM of (10-12) plane (arcsec)	1385	1870	1526	2323	2331	2400

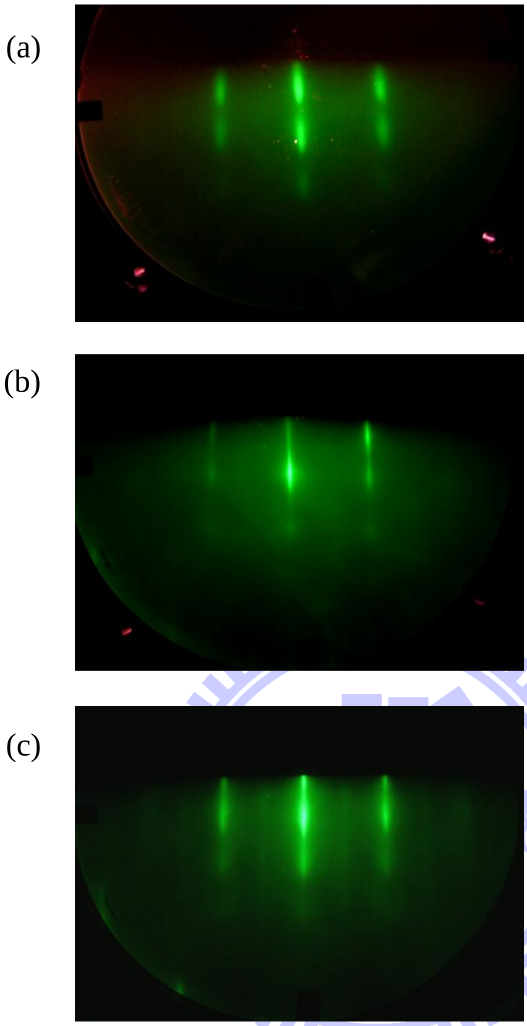

Fig 3.1 Typical RHEED patterns for (a) AlN buffer layer, (b) GaN film during growth and (c) GaN film after cooling.

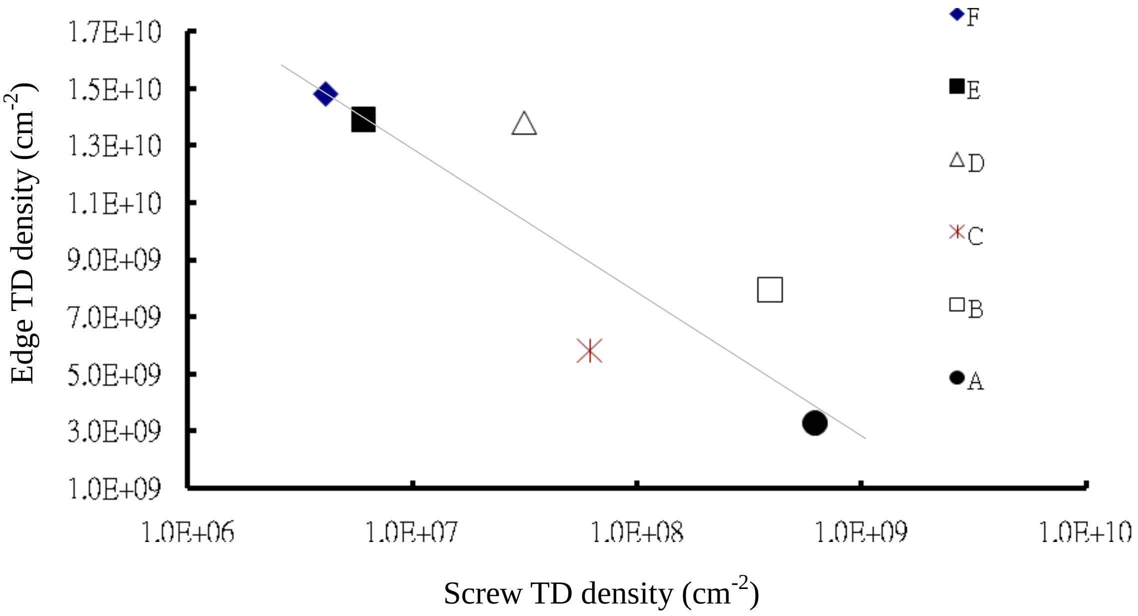

Fig. 3.2 The screw and edge TDs densities of GaN grown on AlN buffer layers with different growth temperatures

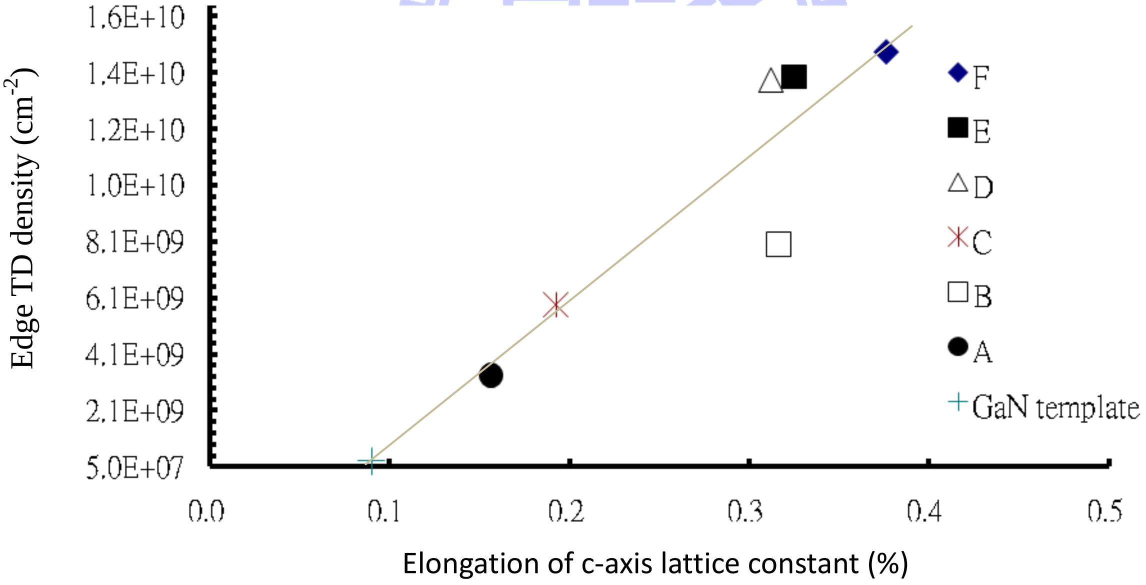

Fig. 3.3 The dependence of edge TD density on the elongation of c-axis lattice constant for the GaN grown on AlN buffer layers prepared at different temperatures.

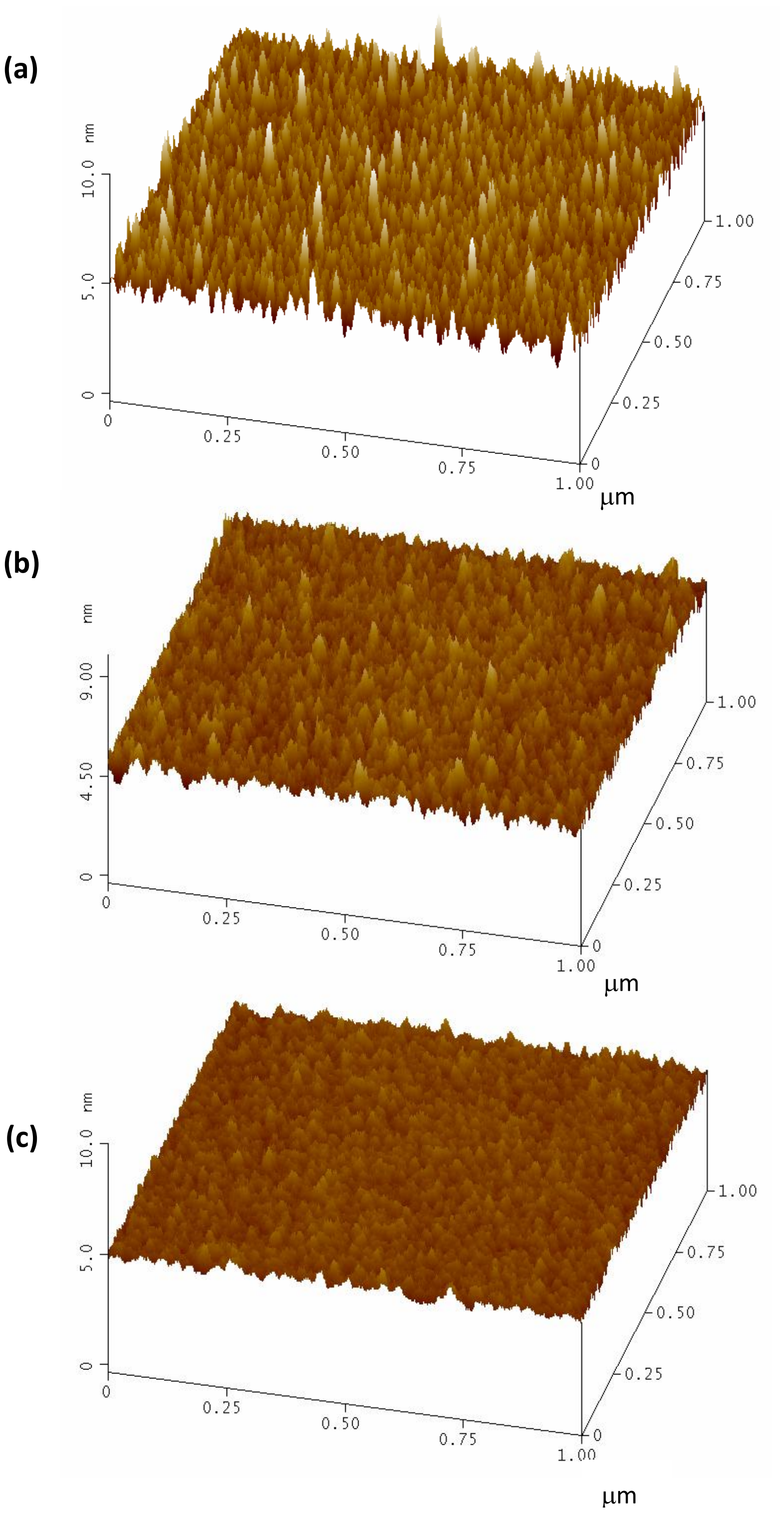

Fig. 3.4 AFM images of AlN buffers grown at temperature (a) 450 °C, (b) 740 °C and (c) 840 °C.

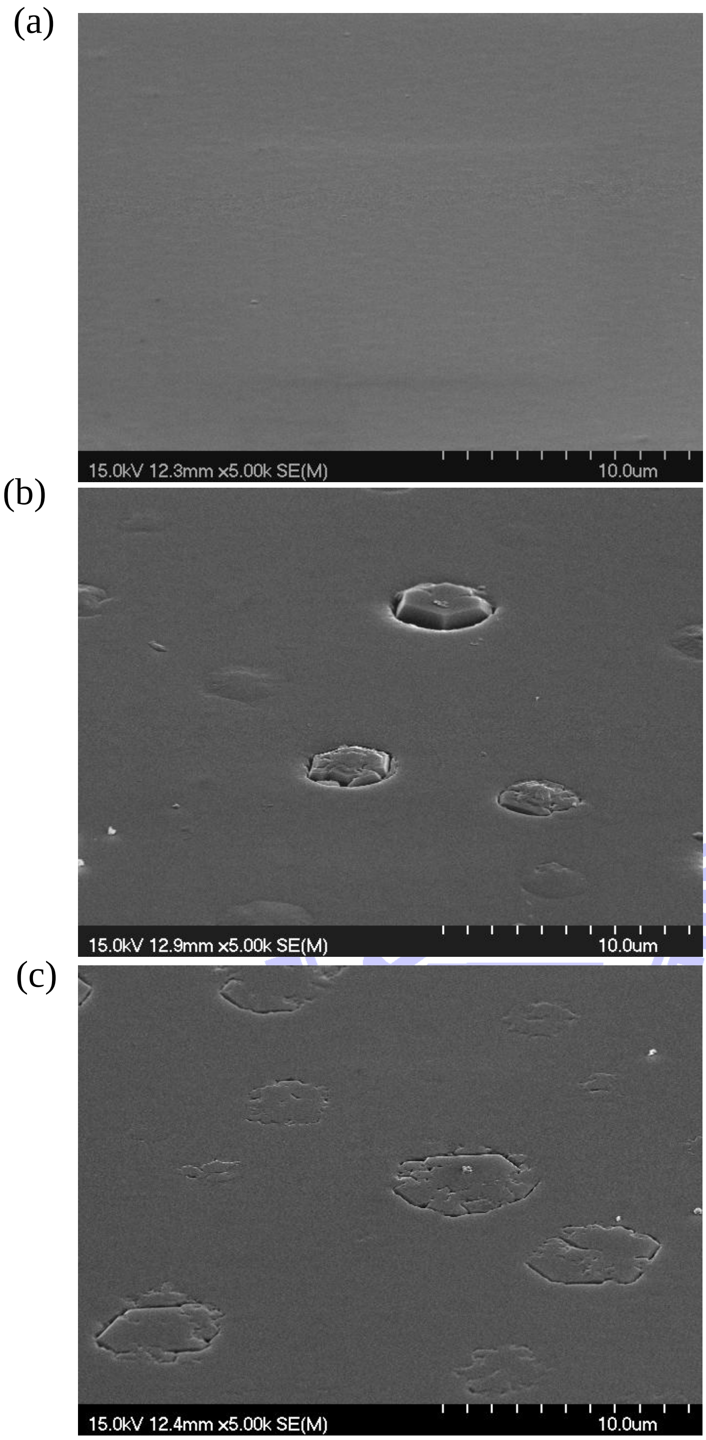

Fig. 3.**5** SEM images of GaN surfaces grown on AlN buffer prepared at (a) 525 °C, (b) 485 °C and (c) 450 °C.

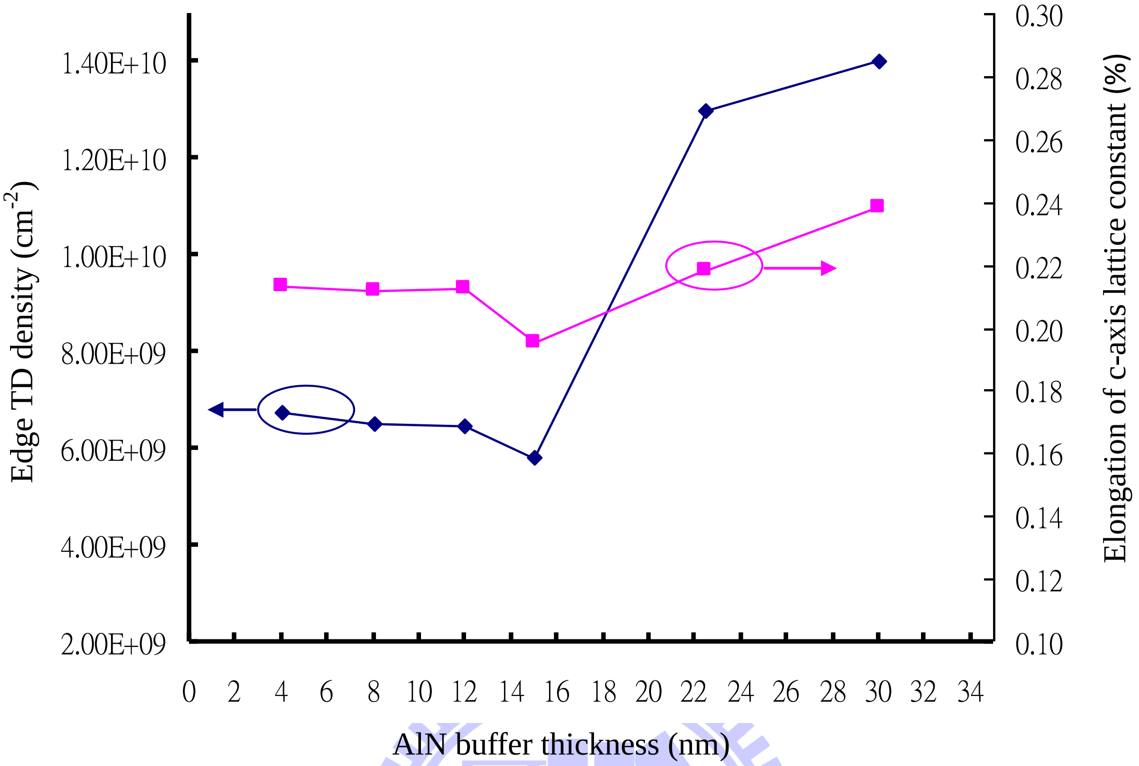

Fig. 3.6 The dependence of the XRD (10-12) FWHM and elongation of c-axis lattice constant on AlN buffer thickness.

Chapter 4

Dislocation reduction in GaN film using Ga-lean GaN buffer and migration enhanced epitaxy

4.1 Introduction

As mentioned in the previous chapters, the buffer layer is important to achieve high crystal quality GaN film on a foreign substrate such as sapphire. Experimental results from Chapter 3 conclude that the surface morphology of AlN buffer will affect the defect structures in the GaN film. Generally, when an AlN of relatively rough surface was used (achieved by lower growth temperature), the edge threading dislocation (TD) density were effectively reduced due to the formation of inclined TDs in the GaN film. However, the screw TD density in the GaN films was increased by this buffer since the rough starting layer would increase the nucleation center for screw dislocation. On the other hand, when an AlN of smooth surface was used, the screw TD density could be minimized but the edge TD in the GaN film would be too high (>10^{10} cm^{-2}) for the fabrication of an useful device. Therefore, a more comprehensive buffer structure should be developed to reduce both the screw and edge TD in the GaN grown on the foreign substrates by MBE.

In this chapter, an additional GaN buffer layer grown at slightly nitrogen stable condition (refer as Ga-lean condition) will be deposited on a smooth AlN buffer layer to reduce the total dislocation density in the GaN film. In this regard, the smooth AlN is used to suppress the formation of screw dislocation while the Ga-lean GaN buffer with a specific surface morphology is used to reduce the edge dislocation density in the GaN film. The Ga-lean buffer exhibits a rough surface with a hill and valley topography which would induce the bending of dislocations and thus promote the dislocation self-interactions. To further enhance the reduction effect, a prolonged growth period of the Ga-lean buffer was prepared to produce a rougher buffer surface. After that, migration enhanced epitaxy (MEE), which is composed of an alternative deposition of Ga atoms and N2 radicals, was employed to recover the rough Ga-lean buffer surface. In this study, the usefulness of MEE to recover a rough GaN surface and the effectiveness of Ga-lean buffer to reduce dislocation density are investigated.

4.2 Experimental procedures

The growth of all epitaxial layers was accomplished using PAMBE (ULVAC MBE System) on sapphire (0001) substrates. The initial growth procedure, namely the thermal cleaning of the substrate, the nitridation, and the growth of a thin AlN (15 nm) buffer layer, was previously described in Chapter 3. After the growth of a thin AlN buffer, the substrate temperature was set to 740 ℃ for the growth of the Ga-lean GaN buffer. During the growth of this layer, the effective flux ratio for Ga/N of ~ 0.75 was used. Here, the effective flux ratio of one is occurred at the point where a rough to smooth transition is seen by RHEED. The Ga-lean buffer was grown to a thickness of ~ 700 nm followed by MEE to recover the rough

Ga-lean buffer surface. During the MEE, Ga atoms and nitrogen radicals were impinged onto the substrate alternatively for 10 seconds in each half-cycle. This was achieved with a programmable logic control (PLC) that has been designed to control the operation of mechanical shutters in front of the growth sources (i.e., Ga and nitrogen radicals). The Ga/N ratio was set to that used to produce a smooth GaN surface, i.e., one during the MEE growth, and the growth temperature was also set at 740℃.

To study the effect of MEE on a rough GaN surface, growth interruptions were introduced. The first growth stop was carried out after the Ga-lean buffer was deposited. The completion of this layer was indicated by the change in RHEED pattern from streaky lines (Fig. 4.1 (a)) to broken, downward arrow lines (Fig. 4.1 (b)). This change suggested that the GaN buffer surface was flat at the beginning and transformed gradually into a rough surface with a specific morphology that will be described later. The sample was removed from the chamber, and the GaN surface morphology was characterized using an atomic force microscope (AFM). Additionally, a high resolution x-ray diffraction (HRXRD) was also used to determine the crystal quality of GaN film. The sample was then cleaned with organic solvents and diluted hydrochloric acid prior to the GaN re-growth using the MEE method. This procedure was repeated several times until the GaN surface was fully recovered. Finally, another GaN layer (~1.5μm), grown with an effective Ga/N ratio of one, was deposited. The total thickness of the sample was approximately 2.5 μm. This sample was designated at Sample A. For comparison, a control sample (Sample B) with a similar thickness but without the Ga-lean buffer was also prepared. In this sample, the GaN layer was grown with an equal Ga/N ratio to one throughout the process. In addition to HRXRD, the crystal quality of these GaN samples was also determined using cross-sectional transmission electron microscopy (TEM). The TEM samples were prepared by cleaving the GaN materials along the (11-20) plane, followed by conventional mechanical polishing and an Ar-ion milling process.

4.3 Results and discussion

4.3.1 Recovering of rough GaN surface by MEE

The evolution of GaN surface morphology in Sample A at different MEE cycles was studied by atomic force microscopy. The AFM measurements (Fig. 4.2 (a)) show that the initial Ga-lean GaN buffer surface was decorated with flat, truncated mesas and deep trenches up to ~100 nm, which correspond with the RHEED pattern shown in Fig. 4.1 (b). After the first 300 cycles of MEE, most of the deep trenches were recovered, and only short, shallow trenches and pits were left (Fig. 4.2 (b)). The RHEED pattern remained less streaky even though the arrow marks vanished. The trenches on the GaN surface were entirely eliminated by an additional 300 MEE cycles (Fig. 4.2 (c)), leaving only small pits on the sample surface. The RHEED pattern appeared to be streaky during the MEE process, but the pattern became less streaky again after the MEE process was stopped and the sample was annealed for a short duration. Finally, the GaN surface was fully recovered (Fig. 4.2 (d)) with an additional 200 MEE cycles. The corresponding RHEED pattern of this smooth GaN was streaky and similar to that shown in Fig. 4.1 (a). The root-mean-square (*rms*) roughness was improved from 24 nm to 0.44 nm. This demonstrates the ability of MEE to recover a rough GaN surface. The roughening of a GaN surface grown under Ga-lean conditions was a result of the low surface diffusivity of adatoms. It has been calculated that the diffusion barrier for Ga adatoms on a highly N-rich surface is as high as 1.8 eV, whereas it is only 0.4 eV on a Ga-saturated surface [52]. It is believed that the diffusion barrier for Ga adatoms on a Ga-lean surface is somewhere between these two values. The reduced mobility of adatoms was responsible for the GaN surface roughening, as shown in an early work by Tarsa et al. [20].

The results suggest one potential mechanism by which MEE recovers the Ga-lean buffer. As illustrated in Fig. 4.3 (a), the inclined trench surfaces on a rough Ga-lean buffer can be represented by a series of steps edges and kinks sites. Due to the abundance of unsaturated bonds, the Gibbs free energy of these sites was higher than that of the flat mesas, which favored adatom residence [53]. During the first MEE half-cycle in which only Ga atoms were deposited, new Ga-N bonds did not form, and the Ga atoms were relatively free to move. They had sufficient time to diffuse along the GaN surface, but most of them would be trapped at the kink sites where the surface energy was higher (Fig. 4.3 (b)). During the second MEE half-cycle, the trapped Ga atoms reacted with nitrogen radicals to form new GaN material

(Fig. 4.3 (c)). On the other hand, nitrogen radicals arrived at the mesa areas without free Ga atoms would stay uncombined and desorbed from the mesa areas. Therefore, the growth rate at trench areas was significantly faster than at the flat mesas, and the GaN surface became smooth after a sufficient number of MEE cycles (Fig. 4.3 (d)).

In our experiments, the MEE half-cycle was relatively long (10 sec), compared with those used by Horikoshi (1 sec, to grow GaAs) [54] or by Lu et al. (2 sec, to grow InN) [55]. This minimized the risk of mechanical failure for the shutters that might be caused by rapid operation. However, this was sufficient to recover the rough GaN surface. The results indicate that, although most of the Ga adatoms had desorbed from flat mesa surface, those Ga adatoms trapped at step edges and kinks sites on the trenches survived until N_2 radicals arrived. In addition, the surface morphology of the GaN film exhibited step-flow growth (Fig. 4.2 (d)). The average surface step height of 0.25 nm, which is very close to the 0.26 nm step height of one (0001) GaN monolayer, was a result of enhanced Ga adatom migration distances on the GaN surface [54]. These results demonstrate the use of MEE as a means to recover a rough GaN surface. The MEE method is commonly used during the growth of GaAs material, and it has been shown to enhance the migration distance of Ga atoms on the GaAs surface [54].

4.3.2 Reduction of dislocation density by Ga-lean GaN buffer

The dislocation density in the GaN film grown on Ga-lean buffer was estimated using XRD scans. Both symmetric (0002) and asymmetric (10-12) x-ray rocking curves were measured from the GaN samples (Fig. 4.4 (a)) and the screw and edge TD densities in GaN film were then calculated adopting the XRD methods as described in Section 2.3.3.1 (Fig 4.4 (b)). The horizontal axis in this figure represents GaN samples after different stages of growth. The displayed values represent the deposition cycles of MEE on Ga-lean buffer, whereas the rightmost one indicates the XRD results of Sample A, with a total GaN thickness of 2.5 μm. The XRD results for Sample B (without Ga-lean GaN buffer, leftmost in Fig. 4.4 (b)) with an FHWM of 113 and 2015 arcsec for (0002) and (10-12) diffractions, respectively, are also included in the figure.

The reduction of TDs, in particular edge TDs, in the GaN material was clearly observed after using the Ga-lean buffer layer, and the TD number continued to decrease when the GaN was grown thicker. This additional reduction was a consequence of dislocation bending and annihilation. Dislocation bending was induced by roughening the GaN surface, which was initiated during the early stages of Ga-lean buffer growth. Dislocation bending brought dislocations closer to each other, allowing them to interact. During these interactions, the edge TDs with Burgers vectors of different signs could be recombined or annihilated [50, 51]. Therefore, the crystal quality was improved with the increase of film thickness because more TD interactions occurred. In Chapter 3, it is shown that when GaN was grown on a rough AlN buffer prepared at low temperature, the edge TD density could be reduced by a similar mechanism. However, the AlN buffer grown at lower temperature also provided many nucleation sites, which acted as origins for screw TDs. Therefore, the number of screw TDs increased significantly. On the other hand, by deposing a Ga-lean GaN layer on the smooth AlN buffer layer, the edge TD density of GaN film was reduced by approximately one order of magnitude from 1.0×10^{10} to 1.4×10^{9} cm^{-2} as estimated by the XRD results despite a slight increase in screw TD density from 1.2×10^{7} to 2.4×10^{7} cm^{-2}. This demonstrates the ability of Ga-lean GaN buffer to reduce edge TDs while suppressing the formation of new screw TDs if the MEE process takes place under optimal conditions which will be discussed below. Fig. 4.2 (a) shows that the Ga-lean surface was 'roughened' by trenches with inclined surfaces rather than by the small three-dimensional mound-like features that could induce new screw dislocation formation. The slight increase in screw TD may be due to the non-optimized MEE process. If some of the Ga atoms deposited on the flat mesa areas of Ga-lean buffer did not diffuse into the trenches or re-evaporate from the surface during the first MEE half-cycle, they would form small GaN clusters upon the arrival of nitrogen radicals. These small GaN clusters would then generate new screw dislocations in the sample. Due to the specific Burgers vector, screw dislocations are difficult to reduce by dislocation bending. Therefore, the screw dislocation density should be kept as low as possible from the beginning of the growth process, and new dislocation formation should be suppressed during growth. A short period of annealing after every MEE half-cycle [55] may be needed to improve the incorporation of Ga atoms into the step and kink sites on the trench areas.

Cross-sectional TEM analysis was used to observe the bending behavior of TDs in GaN films grown on Ga-lean buffer. The dark-field TEM image of Sample A taken under two beam condition with g= [10-10] (Fig. 4.5 (a)) shows an abrupt change of dislocation density from the buffer region (below the dash line) to the GaN film. The boundary of Ga-lean buffer was estimated based on the growth rate of buffer. Under this observation condition, the edge TDs, which are the predominant dislocation type in GaN, and mixed TDs are visible. Fig 4.5 (a) shows that most of the dislocations appeared to be confined within the buffer layer. In contrast, the dislocations in Sample B (Fig. 4.5 (b)) were propagated from the buffer to the GaN surface when a Ga-lean buffer was not used. The traces of TD bending that were discussed in the previous sections were hardly resolved in this region in Sample A because of the high dislocation density in the buffer. However, for material grown above the buffer layer, the TD bending was clearly observed in a higher magnification TEM image taken around the Ga-lean buffer region (Fig. 4.6 (a)). A number of bent TDs (labeled as BTD) were seen interacting with other TDs, and they were then recombined or annihilated via a mechanism similar to the TD reduction mechanisms discussed by Shen et al. [56]. The inclination angles of these bent TDs were between 10^{o} and 50^{o}. A cross-sectional surface profile of the Ga-lean buffer obtained from an AFM image (Fig. 4.2 (a)) is shown in Fig. 4.6 (b). It was found that the trench wall slopes on Ga-lean buffers matched well with the inclination angles of the bent TDs in the TEM image, suggesting that the inclined material surface induced TD bending. Fig.

4.6 (a) shows that the upper region of GaN film is relatively free of dislocations, with the exception of some TDs that grew vertically from the buffer to the sample surface (labeled as VTD). These dislocations might localize to a mesa center on the buffer and they did not interact with any other dislocation during the growth process. In the control sample, all TDs grew in this manner (Fig. 4.5 (b)) because an effective bending mechanism was not present.

From the TEM observations, the TD density in the upper portion of the GaN film in Sample A was ~ $2x10^{8}$ cm^{-2}, which is almost two orders of magnitude lower than in the control sample. This value is also much lower than that reported by Manfra et al. ($5x10^{9}$ cm^{-2}) [10] using a Ga-lean buffer with less significant trenches. This indicates that the dislocation reduction was greatly enhanced with a Ga-lean buffer with deeper trenches. More-prominent dislocation bending and dislocation reduction were both observed in Sample A, compared with in a sample grown on vicinal substrates (TD density ~$4x10^{8}$ cm^{-2} [44]). In this study, discrepancy occurs in the TD densities as estimated using TEM and XRD methods. TEM analysis showed a more pronounced effect of dislocation reduction due to the abrupt changes in TD density from the Ga-lean buffer to the GaN film. On the other hand, the XRD method in this case may over-estimated the dislocation density because its rocking curves values were averaged over the sample thickness. By considering the incident angle of the X-ray applied in this study and the absorption coefficient of GaN material, the penetration depth of the X-ray was estimated to be more than 7 μm [57].

4.4 Conclusions

The usefulness of MEE to recover a rough GaN surface is demonstrated. With MEE, a Ga-lean GaN buffer with deep trenches can be used to enhance the dislocation reduction in a GaN grown by MBE while maintaining the smoothness of the material surface. By using this Ga-lean buffer, the TD density in GaN was reduced by almost two orders of magnitude to $2x10^8$ cm^{-2}. Moreover, the generation of new screw TDs can also be suppressed by this method if the MEE process is optimized. Growth interruptions were applied to investigate the evolutions of the GaN surface morphology and crystal quality under the MEE process. Instead, the whole process can be accomplished inside the MBE chamber by monitoring the change of RHEED pattern. It is shown that, with the combination of a Ga-lean buffer and the MEE method, a high quality GaN material with smooth surface morphology can be grown on a foreign substrate for device applications using MBE with a single growth-run manner.

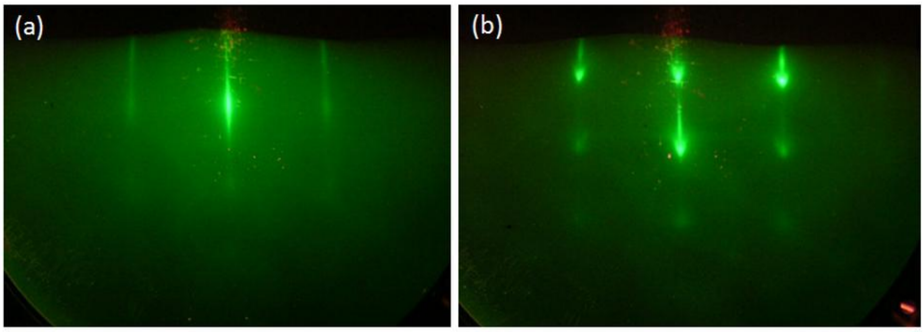

Fig. 4.1 RHEED patterns of **(a)** smooth GaN surface and **(b)** rough Ga-lean GaN buffer surface.

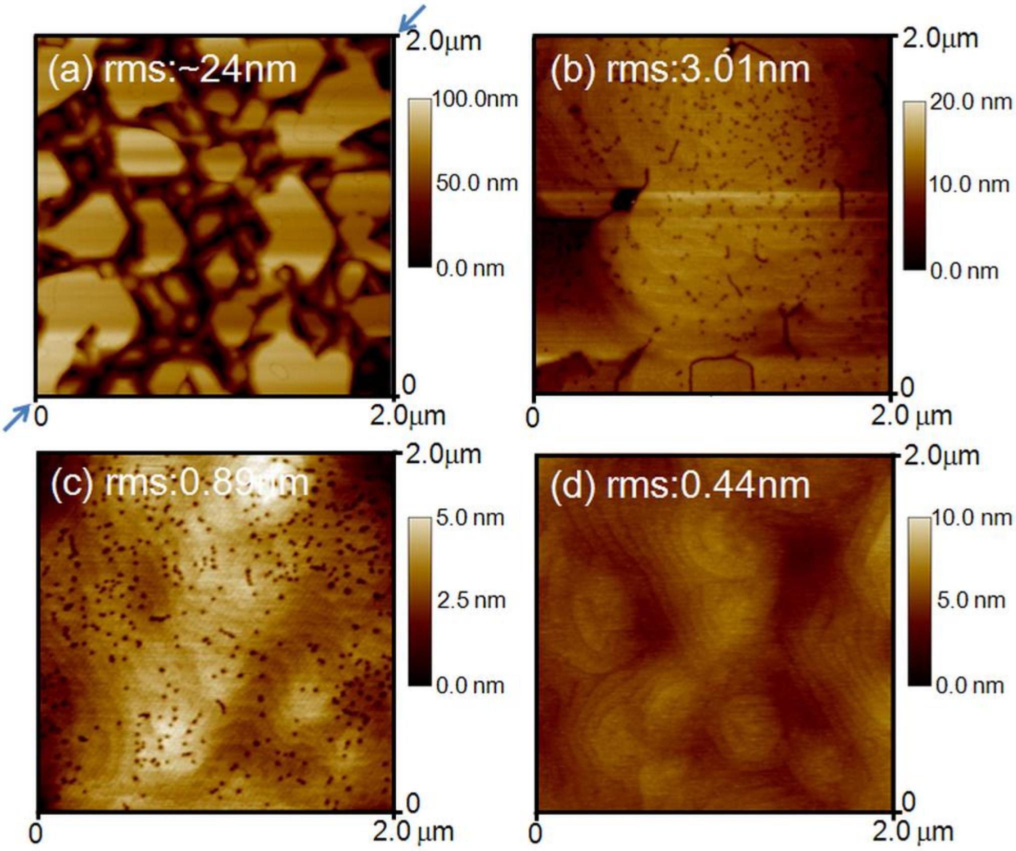

Fig. 4.2 AFM images of the Ga-lean GaN surface after **(a)** 0, **(b)** 300, **(c)** 600 and **(d)** 800 cycles of MEE growth. A cross-sectional profile across the diagonal in image **(a)** (indicated by the arrows) is shown in Fig. 4.6 (b)

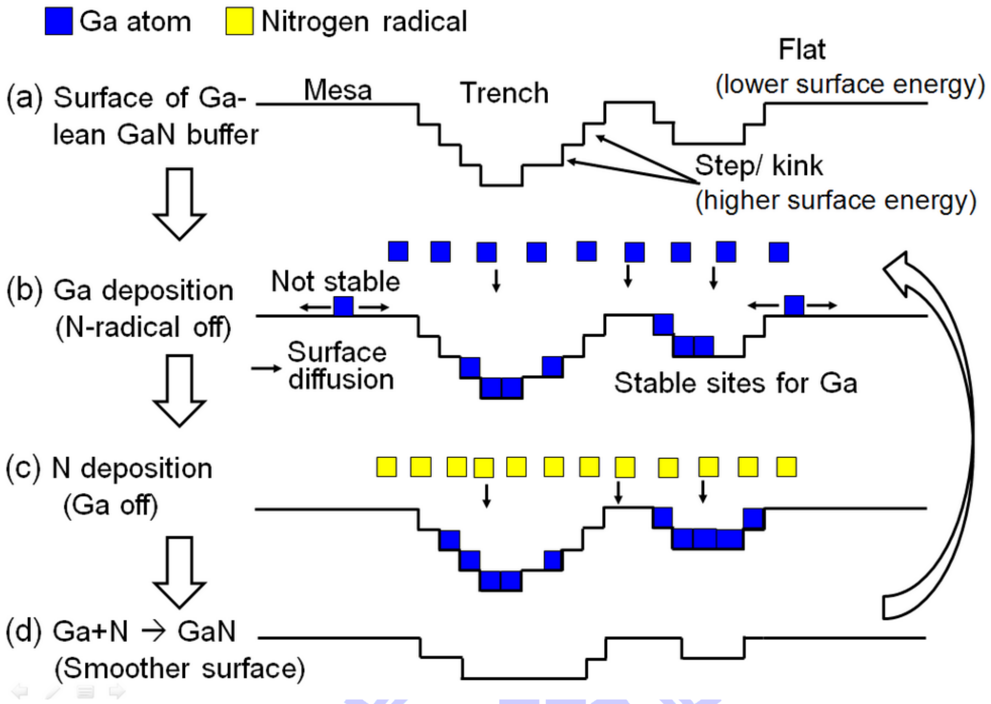

Fig. 4.3 The proposed mechanism of MEE to recover the rough GaN surface grown under Ga-lean condition. **(a)** A Ga-lean GaN buffer surface covered with truncated mesas and deep trenches, **(b)** deposition of Ga atoms during the first half-cycle of MEE, **(c)** deposition of nitrogen radicals during the second half-cycle of MEE, **(d)** a smoother GaN surface after the MEE process.

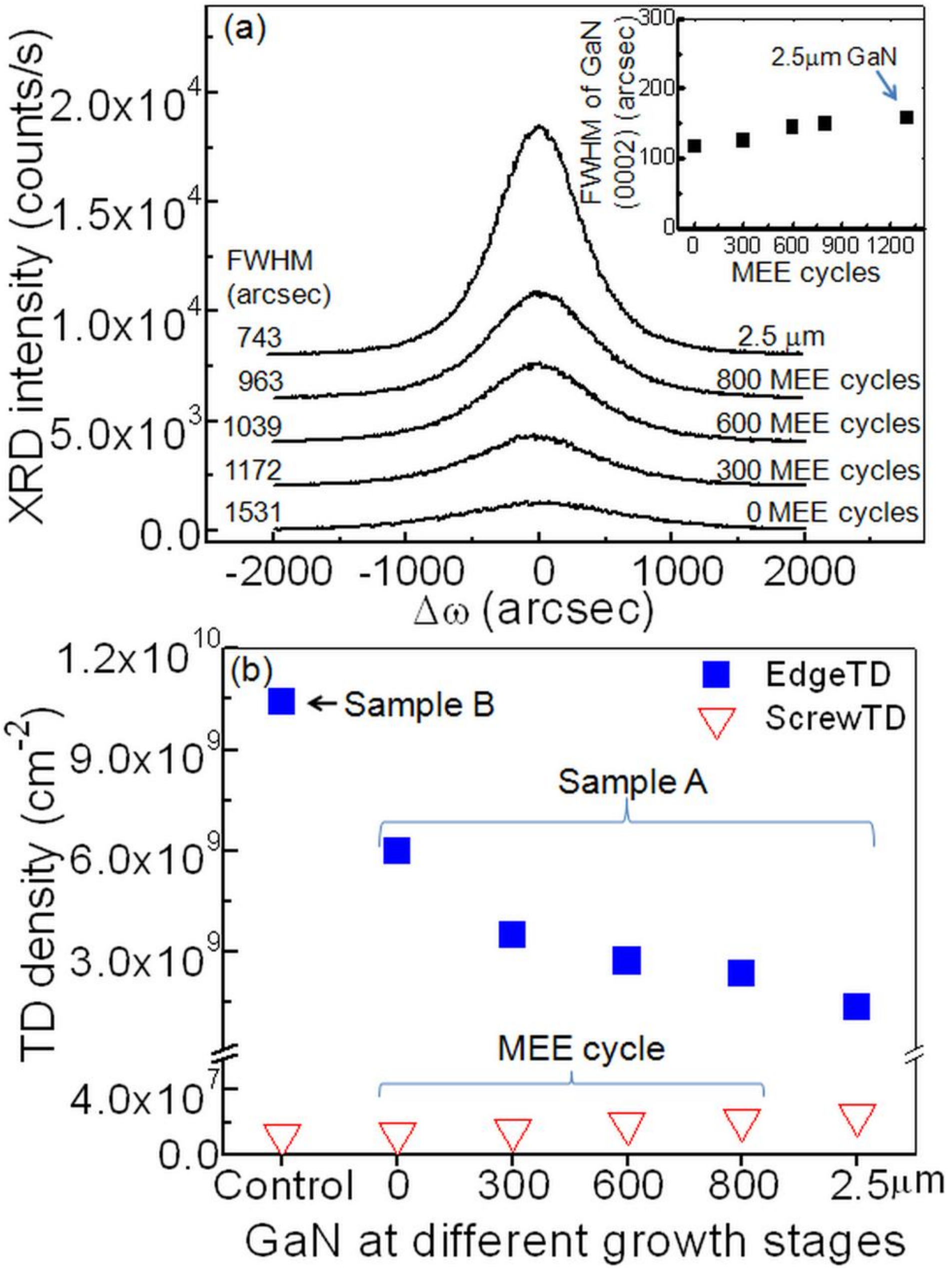

Fig. 4.4 (a) Asymmetric (10-12) rocking curves of the GaN film at different stages of growth. Inset shows the FWHMs of GaN symmetric (0002) deflection peaks after different MEE cycles. **(b)** Estimation of dislocation densities in GaN samples from the XRD results. The ‘2.5µm’ represents the XRD results for the Sample A with 2.5µm GaN film.

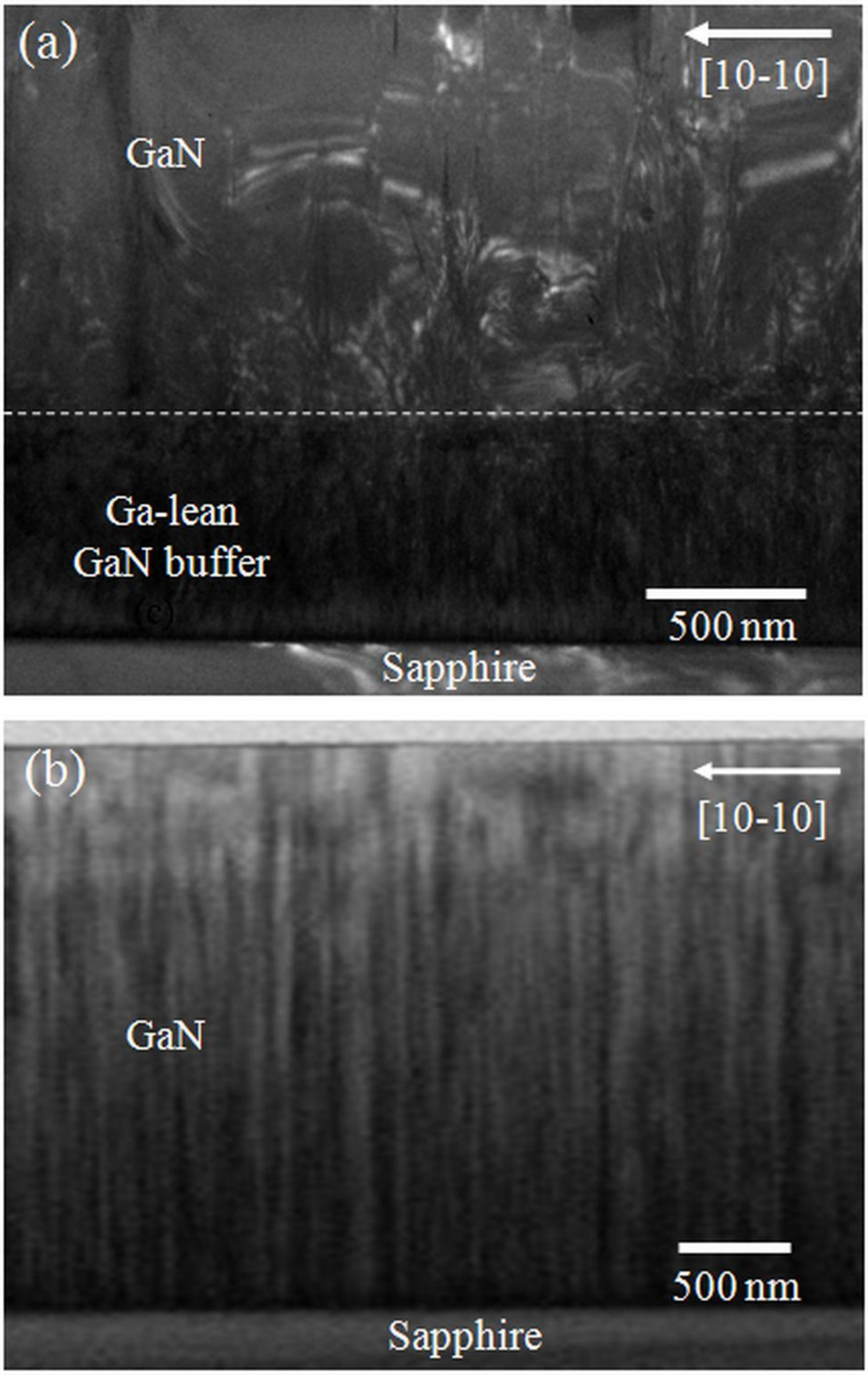

Fig. 4.5 Cross-sectional TEM images of GaN grown **(a)** with and **(b)** without Ga-lean GaN buffer layer. The dashed line in **(a)** shows the boundary between the Ga-lean buffer and GaN film.

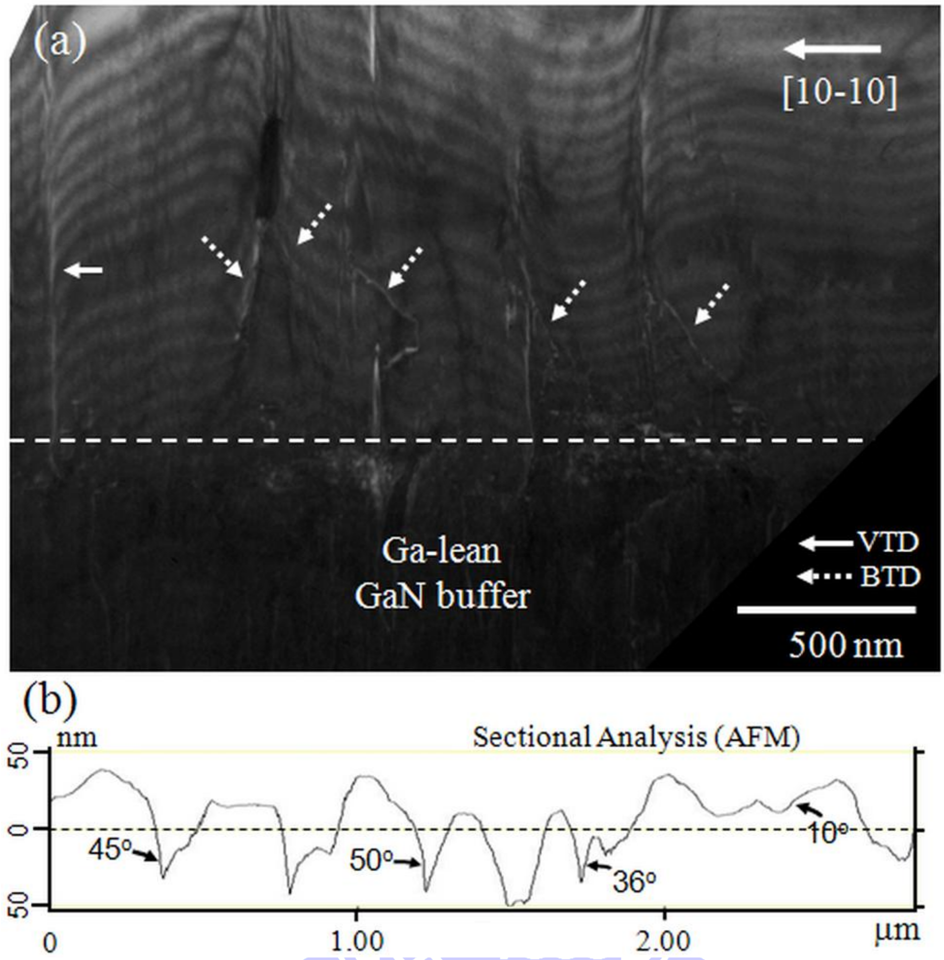

Fig. 4.6 (a) Cross-sectional TEM image of GaN film near the Ga-lean buffer region. The dashed line shows the top of the Ga-lean buffer layer. Arrows indicate the locations of vertical TDs (VTD) and bent TDs (BTD). **(b)** Cross-sectional profile obtained from the AFM image in Fig. 4.2 (a). Some of the slopes on the profile are indicated.

Chapter 5

The Roles of Threading Dislocation on the Electrical Properties of AlGaN/GaN Heterostructure Grown by MBE

5.1 Introduction

GaN high electron mobility transistor (HEMT) devices are excellent candidates for high power and high frequency applications. GaN HEMTs are usually achieved by using either AlGaN or AlInN as the barrier layer on top of a GaN layer. Due to the strong polarization effect and large amount of surface states, high electron density can be induced at the AlGaN/GaN or AlInN/GaN interfaces, as two dimensional electron gas (2DEG) without any intentional doping in the materials. However, as discussed before, the GaN materials grown on a foreign substrate such as sapphire, silicon or silicon carbide are suffering from having high TD density. TDs are known to induce electron scattering in the GaN material, thus reduce the carrier mobility [34, 58, 59], and increase the current leakage path in GaN based devices [60, 61]. High electron mobility in the 2DEG and low reverse-bias leakage current at the gate are the two most important parameters for GaN-based HEMTs to achieve high power performance at high frequency operations. Three types of TDs are normally associated with the hexagonal material of GaN, namely screw type, edge type and mixed type. It is believed that different kinds of TDs may play different roles in the GaN HEMT. However, most of the previous results on dislocation in GaN materials were obtained on the GaN film [58, 62, 63] but did not consider the HEMT devices, while others were measuring the performance of GaN HEMT as a function of total dislocation density [34, 59, 60] but did not take into account the role played by each type of dislocation. In this chapter, the effect of screw and edge TDs on the electrical properties, namely the electron mobility and reverse-bias leakage current of a HEMT structure will be investigated.

5.2 Experimental procedures

The HEMT structures i.e. AlGaN/GaN in this study were all grown by the ULVAC MBE system on sapphire (0001) substrates. The epi-ready substrates were first thermally cleaned in the growth chamber at 820^{o}C until the reflection high-energy electron deflection (RHEED) pattern became streaky. Nitridation of the substrate was then performed at 600^{o}C to form a starting layer for the deposition of AlN buffer and followed by 1.5 micrometer GaN film. In order to prepare GaN film with different defect structure, AlN buffer layer with different growth conditions were prepared (Table 5.1). AlN layer for Sample A to D have the same thickness of 15 nm but grown at different temperature (550 to 800 °C). Meanwhile, for sample M and N, an additional thin Ga-lean GaN buffer was also inserted. On top of all these buffers, initial GaN layer grown under Ga-rich growth condition was first applied to recover the rough surface of these buffer layers. Once the GaN surface became smooth (within tens of nanometers), as indicated by the streaky RHEED patterns, the effective Ga/N ratio was set to slightly larger than unity for the rest of the growth to ensure a smooth surface of GaN layer was maintained. Finally, AlGaN layers with constant Al composition of 25% but with two different thicknesses (20 and 25nm) were grown on the GaN layers.

Atomic force microscopy (AFM) was used to investigate the as-grown sample surfaces. Defect structure of the AlGaN/GaN heterostructures was determined by high-resolution X-ray diffraction (HRXRD) scanning on the rocking curves of different diffraction planes. Aluminum composition and thickness of each AlGaN barrier layers were also determined by HRXRD, using omega-2theta and X-ray reflectivity scan modes, respectively. After the structural characterization, each of the samples was divided into 2 parts and prepared for Hall measurement and Schottky barrier diodes (SBDs) fabrication. From the Hall measurement using Van der Pauw contact configuration, electron mobility, sheet resistance and carrier density of 2DEG were obtained. On the other hand, Schottky barrier diodes (SBDs) fabricated on the AlGaN/GaN samples were used to measure the reverse-bias current. Prior to the fabrication, any metal droplet on the wafer surfaces was removed using diluted hydrochloric acid. The circular SBDs consist of a Schottky contact with diameter of 130 μm at the center of diode, and an ohmic contact formed as the outer ring. Using standard photolithography and lift-off methods, the ohmic contacts of SBD were first fabricated by depositing Ti (200 Å)/Al (1200 Å)/Ni (250 Å)/Au (1000Å) and followed by rapid thermal annealing at 800^{o}C for 1 minute. Then, the Schottky contact was formed by depositing Ni (200 Å)/Au (3000 Å).

5.3 Results and discussion

5.3.1 AFM results

AFM images show the typical surface morphologies of GaN (Fig. 5.1a) and AlGaN (Fig. 5.1b) grown in this study. Surface of AlGaN decorated by small ‘mounds’ is believed to be the result of kinetic roughening in the MBE growth of AlGaN material [64]. The root mean square (rms) roughnesses were 0.44 and 0.65nm, respectively, on a 4 μm^2 area. RHEED patterns of these surfaces are also shown in the insert of each diagram.

5.3.2 Effects of TD on the electron mobility

The dislocation densities of the GaN samples were determined using the HRXRD methods as described in Section 2.3.3.1. X-ray rocking curves (ω-scan) of both symmetric (0002) and asymmetric (10-12) planes were scanned for these samples (Table 5.1). The effects of dislocation in GaN film were compared with the electron mobility obtained from Hall measurements. Fig.5.2 shows the relationship between the electron mobility and edge TD density in AlGaN/GaN samples. It can be seen that the mobility is decreased monotonically with the increase of edge TD density in the samples. For sample D, with edge TD density of more than $1.7x10^{10}$ cm^2, the mobility cannot be measured due to the over-ranged sheet resistance ($>10^6$ ohm/square) and has been set as zero. The reduction of electron mobility in

AlGaN/GaN samples can be explained by considering the edge-type TD as scattering centers for electrons moving in the 2DEG. The dangling bonds along edge dislocation line can act as electron acceptor [58, 59] and filled up with electrons from the channel. Therefore, these negatively charged edge dislocations scattered and reduced the carrier mobility. This is supported by the reduction of sheet carrier density with the increase of edge TD density as shown in Fig. 5.3. All the AlGaN layers were grown under the same growth condition (despite 2 different thicknesses, these thicknesses are well above the critical thickness (~35Å) required to induce carriers into 2DEG [2] from the surface state) and the carrier concentrations induced in the 2DEG are supposed to be similar for all samples. It is the occurrence of trap sites in the dislocations that has reduced the availability of electron as free carriers in the 2DEG. As a result, the measured sheet resistances also increase accordingly. For better illustration of the effect of edge TD, the sheet resistance and free carrier concentration for sample D are set as 10^6 ohm/square and zero, respectively.

In AlGaN/GaN structure, electrons are confined in the 2DEG formed at the close vicinity of heterostructure interface. These carriers are moving parallel to the AlGaN/GaN interface and therefore their mobility can be affected by a variety of factors such as phonon scattering, interface roughness, alloy scattering from the AlGaN barrier and scattering from the charged defects (dislocations, dipoles, residual impurities) [65]. Since the growth condition of AlGaN/GaN is similar for all samples in this experiment, these factors are the invariance properties except the threading dislocation density. The electron mobility is shown to decrease proportionally with the increase of edge TD density, at least in the density range in this study.

On the other hand, there is no clear relationship between the electron mobility and screw TD density (insert of Fig. 5.2). This is understandable since the edge TD densities in all samples are at least 2 orders of magnitude larger than the screw TD densities. For GaN materials grown on sapphire by common methods such as MBE and metal-organic chemical vapor deposition (MOCVD), the dislocation is always dominated by edge TD. The effect of screw dislocation on electron mobility could have been overshadowed by the presence of the large number of edge dislocations. However, it is still reasonable to suggest that the screw TD does not play a significant role in controlling the electron mobility in most of the common cases.

5.3.3 Effects of TD on the reverse-bias leakage current

Another important parameter of HEMT device is the reverse-bias leakage current at the gate contact. This current can be originated from both the surface and bulk material of AlGaN/GaN structure. In this work, only factors controlling the bulk component will be investigated and the surface leakage currents are assumed similar for all samples since they were grown under the same condition. Bulk leakage mechanism play the dominant role in the reverse-bias current [66] and it is believed that the threading dislocation is the major factors controlling this property, as suggested by the literatures [61, 67]. The leakage currents of

AlGaN/GaN structures were determined from the fabricated SBDs. For useful comparison, only sample A, B, C, M and N, with measurable sheet resistances and current densities, have been fabricated into SBDs. Leakage current in SBDs is flowed vertically across the AlGaN layer as in contrast to Hall measurement with electrons moving transversely in the 2DEG. The quality of AlGaN layer is, therefore, crucial under this circumstance. In the present study, crystal qualities of the AlGaN layers are too thin to be determined using HRXRD. Since they were all grown continuously on GaN without applying a growth stop, the dislocations in AlGaN are presumed to be similar to or imitate most of those from the GaN layers. Strain induced from the lattice mismatches between these two materials was believed only to bend TDs slightly in the growth direction but did not obstruct dislocation from propagating to the sample surface. The leakage currents measured at reverse-bias for AlGaN/GaN samples are shown in Fig. 5.4. For sample A, B and C, all with AlGaN thickness of 20nm, the amount of leakage current increases with increasing screw TD density. Insert of Fig. 5.4 shows the values of leakage current measured at the reverse-bias of 5V for these samples. For MBE grown GaN materials, the screw dislocations acted as leakage path for reverse-bias current as suggested by Hsu et al. [61]. Their study also revealed that the screw dislocations, which are likely to be associated with excess Ga under Ga-rich growth condition, have a relaxed core and become electrically active [63]. For sample M and N, with AlGaN thickness of 25nm, their leakage also increased with screw TD density but with much slower rate. This has suggested that the longer leakage paths in thicker AlGaN layers have increased the resistance for leakage current.

On the other hand, the influence of edge TD density on leakage currents is not following a clear trend. At first thought, the availability of free carrier density in the 2DEG (decrease with edge TD density) seems to limit the amount of leakage current as shown in sample A, B and C (with thinner AlGaN layer). But it is not the case for sample M and N (with thicker AlGaN layer). Although the edge TD densities are much higher than the screw TD densities, the role of the latter is dominant in this case. If only sample A, B and C are compared, the slope of the insert of Fig. 5.4 is much steeper than the one in Fig. 5.5. This has suggested that the screw dislocation plays a more important role than the edge dislocation in affecting the reverse-bias leakage current of AlGaN/GaN structure.

5.4 Conclusions

The effects of different TD types on the electrical properties of AlGaN/GaN structure include electron mobility in the 2DEG and reverse-bias leakage current at the gate contact have been investigated. As the dominant type of dislocation in GaN, the edge TD is shown to affect the electron mobility in the 2DEG. They tended to trap carriers in the channel and in turn, acted as the scattering center to reduce the electron mobility. As a result, the availability of free carrier density was reduced while the channel resistance was increased with the increase of the edge TD density. On the other hand, the screw TD seemed not affecting the electron mobility significantly but served as the major player in controlling the reverse-bias leakage current. Each of the screw TD may provide a conducting path in the AlGaN layer for the leakage current and therefore a thicker barrier layer could be used to suppress the leakage current. This is because the current resistance was increased due to the longer leakage paths in the thicker AlGaN layer. The availability of free carrier density in the 2DEG, which is a function of edge TD density, also seems to affect the leakage current for sample with thinner AlGaN layer, but the effect is relatively insignificant as compared to the effect of screw TD density.

Table 5.1 FWHM of GaN (0002) and (10-12) planes prepared on buffers with different growth conditions.

Sample	AlN buffer growth temperature (^{o}C)	FWHM of rocking curve (arcsec)		AlGaN thickness (nm)
		(0002) plane	(10-12) plane	
A	740	71	2404	20
B	700	85	2276	20
C	550	264	1890	20
D	800	75	2584	20
M	800	100	1460	25
N	750	233	1221	25

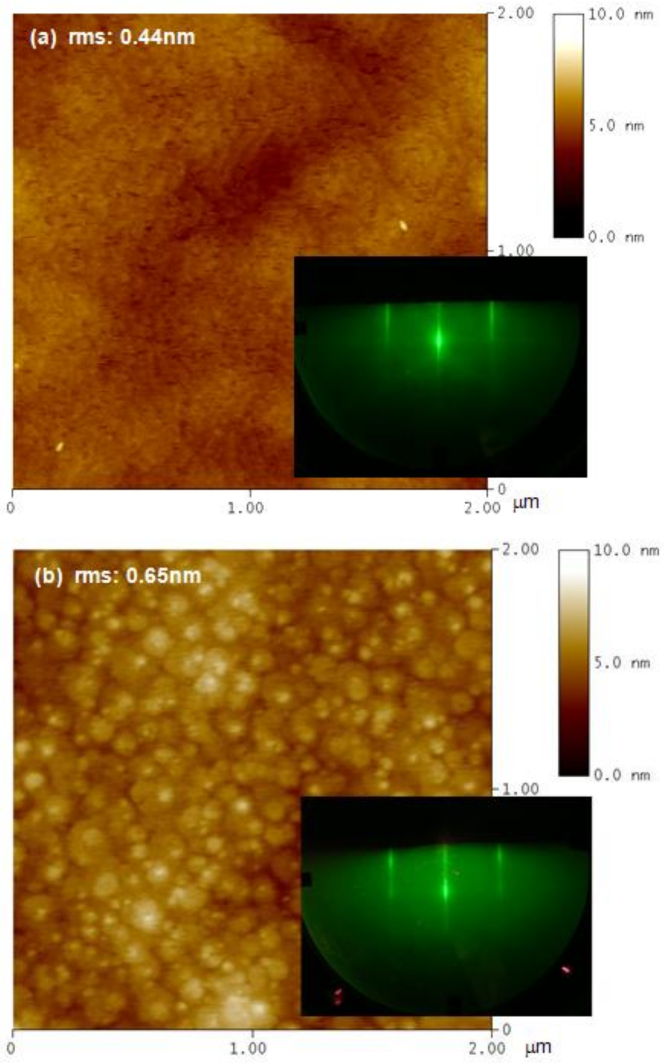

Fig. 5.1 AFM images of the typical as-grown (a) GaN and (b) AlGaN surfaces. Inserts show their corresponding RHEED patterns.

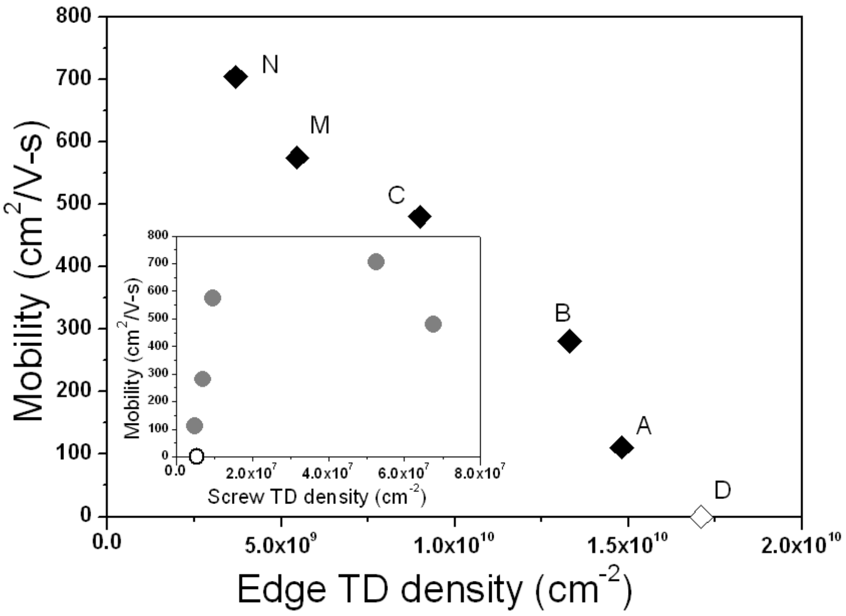

Fig. 5.2. Hall electron mobility of AlGaN/GaN samples as a function of edge TD density. Insert shows the effect of screw TD density on electron mobility. Open symbols in the diagrams represent the values for sample D.

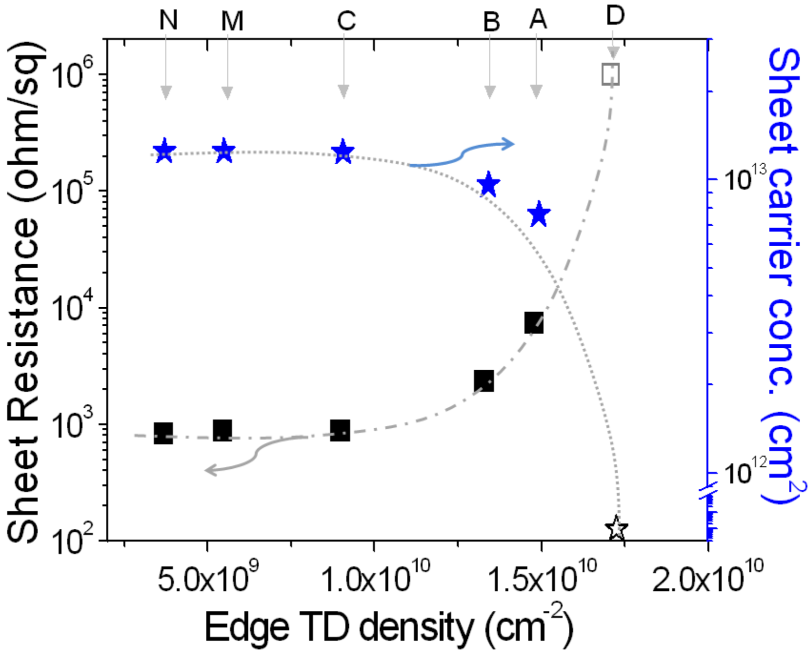

Fig. 5.3. Sheet resistance and carrier concentration of the AlGaN/GaN samples as a function of edge TD density. Open symbols represent the values for sample D.

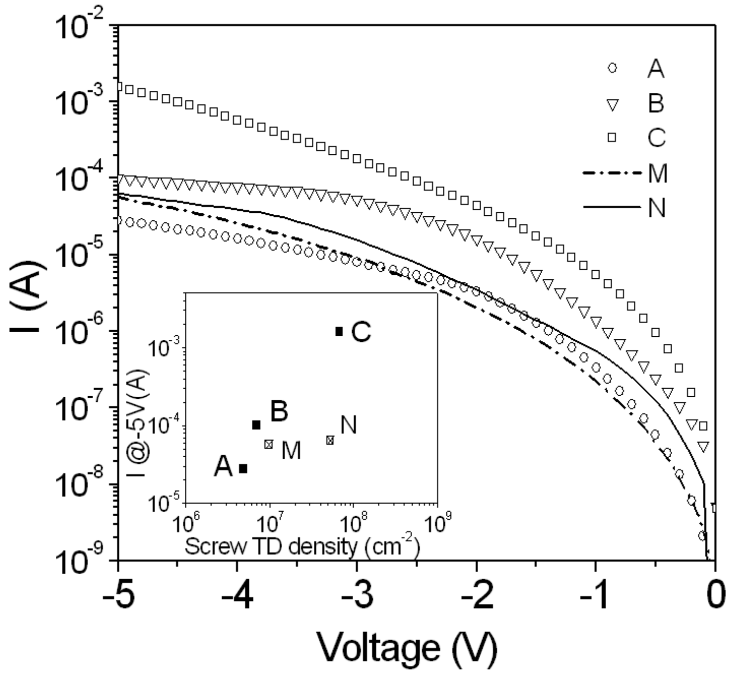

Fig. 5.4. The reverse bias currents of AlGaN/GaN Schottky barrier diode samples. Insert shows the reverse bias current for sample A, B and C at -5V as a function of screw TD.

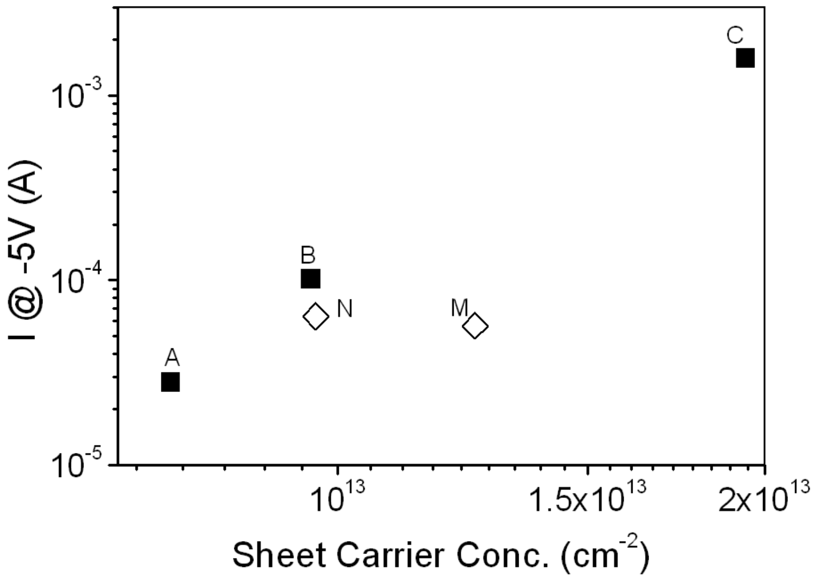

Fig. 5.5. The reverse bias currents of AlGaN/GaN Schottky barrier diode samples as a function of sheet carrier density in the 2DEG.

Chapter 6

Conclusions

The effects of buffer layer structure on the threading dislocation (TD) density in GaN film grown on sapphire by plasma-assisted molecular beam epitaxy (PA-MBE) were investigated. For AlN buffer layer, the growth temperature has contrary effect on the screw and edge TD densities. On a relatively rough AlN surface grown at low temperature (LT), the edge TD density in GaN was reduced through the recombination and annihilation processes of the inclined TDs. However, the screw TD density was increased with the use of lower-temperature AlN because many screw TDs would be generated on the rough buffer surface. Besides, the AlN thickness also affects the TD density especially for the edge TD. More stress and higher edge TD density were generated in the GaN film grown on the AlN with thickness other than the optimum value (15 nm).

An effective method to reduce both screw and edge TDs was also introduced. This method combined an AlN buffer layer grown at high temperature (HT) and a GaN buffer prepared at slightly N-rich condition (Ga-lean condition). The HT-AlN layer minimized the generation of screw TD while the Ga-lean GaN buffer could reduce the edge TD effectively. The Ga-lean GaN surface was covered with truncated mesa separated by deep trenches. The inclined surfaces on the trench walls were found useful in bending the edge TD growth direction to enhance the dislocation recombination and annihilation. As a result, the edge TD density was reduced by approximately two orders of magnitude to $2x10^8$ cm^{-2}. Furthermore, the Ga-lean GaN buffer was suppressed the formation of new screw TDs. The rough surface of Ga-lean buffer was then recovered using migration enhanced epitaxy (MEE), a process of alternating deposition cycle of Ga atoms and N_2 radicals during the MBE growth. By using a sufficient number of MEE cycles, the GaN surface could be fully recovered with atomically-flat morphology.

Finally, the roles of different TDs on the electrical properties of AlGaN/GaN structure were also studied. AlGaN/GaN samples with different defect structures and densities were prepared and measurements were taken from the same sample to study the correlative behaviors of different TDs. The edge TDs tended to trap carriers in the two dimensional electron gas (2DEG) channel to act as Coulomb scattering centers. Therefore, it reduced the carrier mobility and increased the channel resistance. On the other hand, the screw TDs played a much significant role than edge TDs in controlling the reverse-bias leakage current at the gate. Each of the screw TD may provide a conducting path in the AlGaN layer for the leakage current. The leakage current was increased with screw TD density but could be reduce by using thicker AlGaN layer. This is because the current resistance was increased due to the longer leakage paths in such layer.

References

[1] S. Nakamura, "GaN Growth Using GaN Buffer Layer," *Jpn. J. Appl. Phys.*, vol. 30, pp. L1705-L1707, 1991.

[2] J. P. Ibbetson, *et al.*, "Polarization effects, surface states, and the source of electrons in AlGaN/GaN heterostructure field effect transistors," *Appl. Phys. Lett.*, vol. 77, pp. 250-252, 2000.

[3] M. Miyoshi, *et al.*, "Metalorganic Chemical Vapor Deposition and Material Characterization of Lattice-Matched InAlN/GaN Two-Dimensional Electron Gas Heterostructures," *Appl. Phys. Express*, vol. 1, p. 081102, 2008.

[4] A. Chini, *et al.*, "2.1 A/mm current density AlGaN/GaN HEMT," *Electron. Lett.*, vol. 39, pp. 625-626, 2003.

[5] D. Kapolnek, *et al.*, "Structural evolution in epitaxial metalorganic chemical vapor deposition grown GaN films on sapphire," *Appl. Phys. Lett.*, vol. 67, pp. 1541-1543, 1995.

[6] L. Zhou, *et al.*, "Effect of Al/N flux ratio during nucleation layer growth on the microstructure of GaN films grown by molecular-beam epitaxy," *Appl. Phys. Lett.*, vol. 88, p. 011916, 2006.

[7] J. C. Zhang, *et al.*, "The influence of AlN buffer layer thickness on the properties of GaN epilayer," *J. Crys. Growth*, vol. 268, pp. 24-29, 2004.

[8] D. G. Zhao, *et al.*, "Surface morphology of AlN buffer layer and its effect on GaN growth by metalorganic chemical vapor deposition," *Appl. Phys. Lett.*, vol. 85, pp. 1499-1501, 2004.

[9] L. Meshi, *et al.*, "The reduction of threading dislocations in GaN using a GaN nanocolumn interlayer," *Phys. Status Solidi (c)*, vol. 5, pp. 1645-1647, 2008.

[10] M. J. Manfra, *et al.*, "Dislocation and morphology control during molecular-beam epitaxy of AlGaN/GaN heterostructures directly on sapphire substrates," *Appl. Phys. Lett.*, vol. 81, pp. 1456-1458, 2002.

[11] K. Uchida, *et al.*, "Characterization of Double-Buffer Layers and Its Application for the Metalorganic Vapor Phase Epitaxial Growth of GaN," *Jpn. J. Appl. Phys.*, vol. 37, pp. 3882-3888, 1998.

[12] L. K. Li, *et al.*, "High electron mobility AlGaN/GaN heterostructures grown on sapphire substrates by molecular-beam epitaxy," *Appl. Phys. Lett.*, vol. 76, pp. 742-744, 2000.

[13] Y. B. Pan, *et al.*, "Reduction of threading edge dislocation density in n-type GaN by Si delta-doping," *J. Crys. Growth*, vol. 286, pp. 255-258, 2006.

[14] A. E. Romanov, *et al.*, "Modeling the extended defect evolution in lateral epitaxial overgrowth of GaN: Subgrain stability," *J. Appl. Phys.*, vol. 93, pp. 106-114, 2003.

[15] X. Q. Shen, *et al.*, "Quality improvement of III-nitride epilayers and their heterostructures grown on vicinal substrates by rf-MBE," *J. Crys. Growth*, vol. 301-302, pp. 404-409, 2007.

[16] A. Corrion, *et al.*, "Review of Recent Developments in Growth of AlGaN/GaN High-Electron Mobility Transistors on 4H-SiC by Plasma-Assisted Molecular Beam Epitaxy," *IEICE Trans Electron* vol. E89-C, pp. 906-912, 2006.

[17] X. H. Wu, *et al.*, "Dislocation generation in GaN heteroepitaxy," *J. Cryst. Growth*, vol. 189/190, pp. 231-243 1998.

[18] O. Ambacher, *et al.*, "Two-dimensional electron gases induced by spontaneous and piezoelectric polarization charges in N- and Ga-face AlGaN/GaN heterostructures," *J. Appl. Physics*, vol. 85, pp. 3222-3233, 1999.

[19] M. Sumiya and S. Fuke, "Review of polarity determination and control of GaN," *MRS Internet J. Nitride Semicond. Res.*, vol. 9, pp. 1-34, 2004.

[20] E. J. Tarsa, *et al.*, "Homoepitaxial growth of GaN under Ga-stable and N-stable conditions by plasma-assisted molecular beam epitaxy," *J. Appl. Phys.*, vol. 82, pp. 5472-5479, 1997.

[21] N. Newman, "Thermochemistry of III-N Semiconductors," in *Gallium Nitride (GaN) I*

J. I. Pankove and T. D. Moustakas, Eds., ed: Academic Press, 1999, pp. 55-101.

[22] B. Heying, *et al.*, "Control of GaN surface morphologies using plasma-assisted molecular beam epitaxy," *J. Appl. Phys.*, vol. 88, pp. 1855-1860, 2000.

[23] R. Gaska, *et al.*, "Electron mobility in modulation-doped AlGaN--GaN heterostructures," *Appl. Phys. Lett.*, vol. 74, pp. 287-289, 1999.

[24] M. Higashiwaki, *et al.*, "AlGaN/GaN Heterostructure Field-Effect Transistors on

4H-SiC Substrates with Current-Gain Cutoff Frequency of 190 GHz," *Appl. Phys. Express*, vol. 1, pp. 021103-1, 2008.

[25] T. Wang, *et al.*, "Electron mobility exceeding 10^4 cm^2/V s in an AlGaN--GaN heterostructure grown on a sapphire substrate," *Appl. Phys. Lett.*, vol. 74, pp. 3531-3533, 1999.

[26] J. Liu, *et al.*, "AlGaN/GaN/InGaN/GaN DH-HEMTs with an InGaN notch for enhanced carrier confinement," *IEEE Electron Device Lett.*, vol. 27, pp. 10-12, 2006.

[27] R. Tulek, *et al.*, "Comparison of the transport properties of high quality AlGaN/AlN/GaN and AlInN/AlN/GaN two-dimensional electron gas heterostructures," *J. Appl. Phys.*, vol. 105, p. 013707, 2009.

[28] J. Selvaraj, *et al.*, "Effect of GaN Buffer Layer Growth Pressure on the Device Characteristics of AlGaN/GaN High-Electron-Mobility Transistors on Si," *Jpn. J. Appl. Phys.*, vol. 48, 2009.

[29] S. Arulkumaran, *et al.*, "Low Specific On-Resistance AlGaN/AlN/GaN High Electron Mobility Transistors on High Resistivity Silicon Substrate," *Electrochem. Solid-State Lett.*, vol. 13, pp. H169-H172, 2010.

[30] D. C. Dumka, *et al.*, "AlGaN/GaN HEMTs on Si substrate with 7 W/mm output power density at 10 GHz," *Electronics Lett.*, vol. 40, pp. 1023-1024, 2004.

[31] C. R. Elsass, *et al.*, "Electron Transport in AlGaN/GaN Heterostructures Grown by Plasma-Assisted Molecular Beam Epitaxy," *Jpn. J. Appl. Phys.*, vol. 39, pp. L1023-L1025, 2000.

[32] Y. Cordier, *et al.*, "AlGaN/GaN HEMTs regrown by MBE on epi-ready semi-insulating GaN-on-sapphire with inhibited interface contamination," *J. Crys. Growth*, vol. 309, pp. 1-7, 2007.

[33] M. J. Manfra, *et al.*, "Electron mobility in very low density GaN/AlGaN/GaN heterostructures," *Appl. Phys. Lett.*, vol. 85, pp. 1722-1724, 2004.

[34] C. Skierbiszewski, *et al.*, "High mobility two-dimensional electron gas in AlGaN/GaN heterostructures grown on bulk GaN by plasma assisted molecular beam epitaxy," *Appl. Phys. Lett.*, vol. 86, p. 102106, 2005.

[35] S.-G. Shen, "Study of GaN Epitaxial Growth on Sapphire (0001) and Silicon (111) Substrates by Molecular Beam Epitaxial System," Master of Electronics Engineering,

Electronics Engineering, National Chiao Tung University, Hsinchu, Taiwan, 2007.

[36] M. Stutzmann, *et al.*, "Playing with Polarity," *Phys. Stat. Solidi (b)*, vol. 228, pp. 505-512, 2001.

[37] B. Heying, *et al.*, "Optimization of the surface morphologies and electron mobilities in GaN grown by plasma-assisted molecular beam epitaxy," *Appl. Phys. Lett.*, vol. 77, pp. 2885-2887, 2000.

[38] A. R. Smith, *et al.*, "Determination of wurtzite GaN lattice polarity based on surface reconstruction," *Appl. Phys. Lett.*, vol. 72, pp. 2114-2116, 1998.

[39] B. Heying, *et al.*, "Role of threading dislocation structure on the x-ray diffraction peak widths in epitaxial GaN films," *Appl. Phys. Lett.*, vol. 68, pp. 643-645, 1996.

[40] P. Gay, *et al.*, "The Estimation of Dislocation Densities in Metals from X-ray Data," *Acta Metall.*, vol. 1, pp. 315-319, 1953.

[41] G. Koblmueller, *et al.*, "Growth diagram and morphologies of AlN thin films grown by molecular beam epitaxy," *J. Appl. Physics*, vol. 93, pp. 9591-9596, 2003.

[42] V. S. Harutyunyan and et al., "High-resolution x-ray diffraction strain-stress analysis of GaN/sapphire heterostructures," *J. Phys. D: Appl. Phys.*, vol. 34, p. A35, 2001.

[43] X.-Q. Shen, *et al.*, "Impact of Vicinal Sapphire (0001) Substrates on the High-Quality AlN Films by Plasma-Assisted Molecular Beam Epitaxy," *Jpn. J. Appl. Phys.*, vol. 42, pp. L1293-L1295, 2003.

[44] X. Q. Shen, *et al.*, "Reduction of the threading dislocation density in GaN films grown on vicinal sapphire (0001) substrates," *Appl. Phys. Lett.*, vol. 86, p. 021912, 2005.

[45] A. Trampert, *et al.*, "Crystal Structure of Group III Nitrides," in *Gallium Nitride (GaN) I*, J. I. Pankove and T. D. Moustakas, Eds., ed: Academic Press, 1999, pp. 167-192.

[46] J. Keckes, *et al.*, "Temperature dependence of stresses in GaN/AlN/6H–SiC(0001) structures: correlation between AlN buffer thickness and intrinsic stresses in GaN," *J. Crys. Growth*, vol. 246, pp. 73-77, 2002.

[47] L. Sugiura, "Dislocation motion in GaN light-emitting devices and its effect on device lifetime," *J. Appl. Phys.*, vol. 81, pp. 1633-1638, 1997.

[48] Y. Kim, *et al.*, "GaN thin films by growth on Ga-rich GaN buffer layers," *J. Appl. Phys.*, vol. 88, pp. 6032-6036, 2000.

[49] P. Cantu, *et al.*, "Si doping effect on strain reduction in compressively strained Al[sub 0.49]Ga[sub 0.51]N thin films," *Appl. Phys. Lett.*, vol. 83, pp. 674-676, 2003.

[50] P. Waltereit, *et al.*, "Structural Properties of GaN Buffer Layers on 4H-SiC(0001) Grown by Plasma-Assisted Molecular Beam Epitaxy for High Electron Mobility Transistors," *Jpn. J. Appl. Phys.*, vol. 43, pp. L1520-L1523, November 5, 2004 2004.

[51] C. D. Lee, *et al.*, "Role of Ga flux in dislocation reduction in GaN films grown on SiC(0001)," *Appl. Phys. Lett.*, vol. 79, pp. 3428-3430, 2001.

[52] T. Zywietz, *et al.*, "Adatom diffusion at GaN (0001) and (0001-bar) surfaces," *Appl. Phys. Lett.*, vol. 73, pp. 487-489, 1998.

[53] I. V. Markov, "Crystal-Ambient Phase Equilibrium," in *Crystal growth for beginners. Fundamentals of nucleation, crystal growth and epitaxy*, 2nd ed: World Scientific, 2003, pp. 1-75.

[54] Y. Horikoshi, "Advanced epitaxial growth techniques: atomic layer epitaxy and migration-enhanced epitaxy," *J. Crys. Growth*, vol. 201-202, pp. 150-158, 1999.

[55] H. Lu, *et al.*, "Improvement on epitaxial grown of InN by migration enhanced epitaxy," *Appl. Phys. Lett.*, vol. 77, pp. 2548-2550, 2000.

[56] X. Q. Shen, *et al.*, "Studies of the annihilation mechanism of threading dislocation in AlN films grown on vicinal sapphire (0001) substrates using transmission electron microscopy," *Appl. Phys. Lett.*, vol. 87, p. 101910, 2005.

[57] A. Reiher, *et al.*, "Depth-resolving structural analysis of GaN layers by skew angle x-ray diffraction," *Appl. Phys. Lett.*, vol. 84, pp. 3537-3539, 2004.

[58] J. H. You, *et al.*, "Electron scattering due to threading edge dislocations in n-type wurtzite GaN," *J. Appl. Phys.*, vol. 99, p. 033706, 2006.

[59] N. G. Weimann, *et al.*, "Scattering of electrons at threading dislocations in GaN," *J. Appl. Phys.*, vol. 83, pp. 3656-3659, 1998.

[60] K. H. Lee, *et al.*, "AlGaN/GaN Schottky Barrier Diodes with Multi-Mg_xN_y/GaN Buffer," *J. Electrochem Soc.*, vol. 155, pp. H716-H719, 2008.

[61] J. W. P. Hsu, *et al.*, "Inhomogeneous spatial distribution of reverse bias leakage in GaN Schottky diodes," *Appl. Phys. Lett.*, vol. 78, pp. 1685-1687, 2001.

[62] P. Ebert, *et al.*, "Electronic properties of dislocations in GaN investigated by scanning

tunneling microscopy," *Appl. Phys. Lett.*, vol. 94, p. 062104, 2009.

[63] J. W. P. Hsu, *et al.*, "Effect of growth stoichiometry on the electrical activity of screw dislocations in GaN films grown by molecular-beam epitaxy," *Appl. Phys. Lett.*, vol. 78, pp. 3980-3982, 2001.

[64] S. Vézian, *et al.*, "From spiral growth to kinetic roughening in molecular-beam epitaxy of GaN(0001)," *Phys. Rev. B,* vol. 69, p. 125329, 2004.

[65] D. Jena, "Polarization Effects on Low-Field Transport & Mobility in III-V Nitride HEMTs," in *Polarization Effects in Semiconductors, From Ab InitioTheory to Device Applications*, *C. Wood* and *D. Jena*, Eds., 1st edition ed: Springer, 2007, pp. 161-216.

[66] W. S. Tan and P. A. Houston, "Understanding Surface and Bulk Leakage Mechanisms in AlGaN/GaN HFETs," in *2nd EMRS DTC Technical Conference*, Edinburgh, 2005, p. A27.

[67] E. J. Miller, *et al.*, "Analysis of reverse-bias leakage current mechanisms in GaN grown by molecular-beam epitaxy," *Appl. Phys. Lett.*, vol. 84, pp. 535-537, 2004.

Vita

Name：Yuen-Yee Wong (黃延儀)

Gender: Male

Date of Birth: 10 Aug 1975

Nationality: Malaysian

Email: yuenyee98.mse94g@nctu.edu.tw; yuenyee98@yahoo.com

Education Background

1. Doctor of Philosophy, Materials Science and Engineering, National Chiao Tung University, Taiwan (Feb 2006 – July 2011)
2. Master of Science, Applied Physics, University of Malaya, Malaysia (July 2000 – August 2003)
3. Bachelor of Science, Applied Physics, University of Malaya, Malaysia (July 1996 – September 1999)

Thesis of Doctor of Philosophy:

Epitaxial Growth of AlGaN/GaN Heterostructure by Plasma-assisted Molecular Beam Epitaxy for High Electron Mobility Transistor Applications

(以電漿輔助式分子束磊晶成長應用於高電子遷移率電晶體之氮化鋁鎵/氮化鎵異質結構)

Publication List

A. Patents

1. Yuen-Yee Wong and Edward Yi Chang, ***A method for reducing defects in epitaxially grown on group III-nitride materials process***. Patents are applying in Taiwan R.O.C. and United States of America. 交通大學 09(專)A076; 和宸智權 S98024_TW, S98024_US.

B. Journal Papers

1. Trinh, H. D.; Brammertz, G.; Chang, E. Y.; Kuo, C. I.; Lu, C. Y.; Lin, Y. C.; Nguyen, H. Q.; Wong, Y. Y.; Tran, B. T.; Kakushima, K.; Iwai, H., ***Electrical Characterization of Al_2O_3/n-InAs Metal–Oxide–Semiconductor Capacitors With Various Surface Treatments***, Electron Device Letters, IEEE , vol.32, no.6, pp752-754, 2011.

2. Yuen-Yee Wong, Edward Yi Chang, Yue-Han Wu, Mantu K. Hudait, Tsung-Hsi Yang, Jet-Rung Chang, Jui-Tai Ku, Wu-Ching Chou, Chiang-Yao Chen, Jer-Shen Maa, Yueh-Chin Lin, ***Dislocation reduction in GaN film using Ga-lean GaN buffer layer and migration enhanced epitaxy***, Journal of Thin Solid Film, vol. 509, issue 19, pp 6208-6213, 2011.

3. Yu, H. W., Chang, E. Y., Nguyen, H. Q., Chang, J. T., Chung, C. C., Kuo, C. I., Wong, Y. Y., Wang, W. C., ***Effect of substrate misorientation on the material properties of GaAs/Al0.3Ga0.7As tunnel diodes***, Applied Physics Letters, vol.97, no.23, 231903, 2010.

4. Lin, Y. C. , Shie, S.-L., Shie, T.-E., Wong, Y.-Y., Chen, K.S., Chang, E.Y., ***Study of the formation mechanism of Cu/Ge/Pd ohmic contact to n-type InGaAs.*** Journal of Electronic Materials, vol. 40, issue 3, pp 289-294, 2010**.**

5. Hai-Dang Trinh, Edward Yi Chang, Yuen-Yee Wong, Chih-Chieh Yu, Chia-Yuan Chang, Yueh-Chin Lin, Hong-Quan Nguyen and Binh-Tinh Tran, ***Effects of Wet Chemical and Trimethyl Aluminum Treatments on the Interface Properties in Atomic Layer Deposition of Al_2O_3 on InAs.*** Japanese Journal of Applied Physics, 49, 111201, 2010.

6. H. D. Trinh, E. Y. Chang, P. W. Wu, Y. Y. Wong, C. T. Chang, Y. F. Hsieh, C. C. Yu, H. Q. Nguyen, Y. C. Lin, K. L. Lin, and M. K. Hudait, ***The influences of surface treatment and gas annealing conditions on the inversion behaviors of the atomic-layer-deposition Al_2O_3 /n-$In_{0.53}Ga_{0.47}$As metal-oxide-semiconductor capacitor***. Applied Physics Letter, 97, 042903, 2010.

7. Yuen-Yee Wong, Edward Yi Chang, Tsung-Hsi Yang, Jet-Rung Chang, Jui-Tai Ku, Wu-Ching Chou, Micheal Chen and Kung-Liang Lin. ***The Roles of Threading Dislocations on Electrical Properties of AlGaN/GaN Heterostructure Grown by MBE***. Journal of the Electrochemical Society, 157, pp H746-H749, 2010.

8. Kung-Liang Lin, Edward-Yi Chang, Yu-Lin Hsiao, Wei-Ching Huang, Tien-Tung Luong, Yuen-Yee Wong, Tingkai Li, Doug Tweet, and Chen-Hao Chiang, ***Effects of Al$_x$Ga$_{1-x}$N interlayer for GaN epilayer grown on Si substrate by metal-organic chemical-vapor deposition.*** Journal of Vacuum Science and Technology B. 28, pp 473-477, May 2010.

9. Jui-Tai Ku, Tsung-Hsi Yang, Jet-Rung Chang, Yuen-Yee Wong, Wu-Ching Chou, Chun-Yen Chang and Chiang-Yao Chen, ***Epitaxial overgrowth of gallium nitride nano-rods on silicon (111) substrates by RF-plasma-assisted molecular beam epitaxy***. Japanese Journal of Applied Physics 49, 04DH06, 2010.

10. Yun-Chi Wu, Edward Yi Chang, Yueh-Chin Lin, Chi-Chung Kei, Mantu K. Hudait, Marko Radosavljevic, Yuen-Yee Wong, Chia-Ta Chang, Jui-Chien Huang, Shih-Hsuan Tang, ***Study of the inversion behaviors of Al$_2$O$_3$/In$_x$Ga$_{1-x}$As metal–oxide–semiconductor capacitors with different In contents***. Solid-State Electronics, 54, pp 37–41, 2010.

11. Yuen-Yee Wong, Edward Yi Chang, Tsung-Hsi Yang, Jet-Rung Chang, Yi-Cheng Chen and Jui-Tai Ku, ***The Effect of AlN Buffer Growth Parameters on the Defect Structure of GaN Grown on Sapphire by Plasma-assisted Molecular Beam Epitaxy.*** Journal of Crystal Growth, 311, pp 1487-1492, 2009.

12. Tsung Hsi Yang, Jui Tai Ku, Jet-Rung Chang, Shih-Guo Shen, Yi-Cheng Chen, Yuen Yee Wong, Wu Ching Chou, Chien-Ying Chen and Chun-Yen Chang, ***Growth of free-standing GaN layer on Si(1 1 1) substrate.*** Journal of Crystal Growth, 311, pp 1997-2001, 2009.

13. Jet Rung Chang, Tsung Hsi Yang, Jui Tai Ku, Shih Guo Shen, Yi Cheng Chen, Yuen Yee Wong, and Chun Yen Chang, ***GaN Growth on Si(111) Using Simultaneous AlN/α-Si3N4 Buffer Structure***. Japanese Journal of Applied Physics, vol. 47, no. 7, pp 5572–5575, 2008.

14. Kartika Chandra Sahoo, Chun-Wei Chang, Yuen-Yee Wong, Tung-Ling Hsieh, Edward Yi Chang, and Ching-Ting Lee, ***Novel Cu/Cr/Ge/Pd Ohmic Contacts on Highly Doped n-GaAs.*** Journal of Electronic Materials, vol. 37, no. 6, pp 901-904, 2008.

C. Conference Proceedings

1. C. F. Dee, Y. Y. Wong, K. P. Lim and B. Y. Majlis, ***Study of the thermal property of copper oxide nanowires.*** Proc. of SPIE Vol. 7493, 749346 (2009), pp 1-5, 2009.

2. Chang, J.-R. , Yang, T. H. , Chen, Y.-C. , Ku, J. T. , Wong, Y. Y. , Chang, C.-Y., ***"Growth and Characterization of MBE-GaN on Si (111) using AlN/α-Si3N4 Buffer Structure"***, 213th ECS Meeting pp. 29-37 Volume 13, Issue 3 - May 18 - May 23, 2008 , Phoenix, AZ. State-of-the-Art Program on Compound Semiconductors 48 (SOTAPOCS 48) -and- ZnO, InZnO, and InGaO Related Materials and Devices for Electronic and Photonic Applications, Editor(s): M. Overberg, F. Ren, B. Gila, H. Ouyang, P. Nam, L. Chen, J. Kim, J. LaRoche

3. Yuen-Yee Wong, Edward Yi Chang, Tsung-His Yang, Jet-Rung Chang, Yi-Cheng Chen and Jui-Tai Ku, 2008. ***Dependence of GaN Defect Structure on the Growth Temperature of the AlN Buffer Layer.*** Mater. Res. Soc. Symp. Proc. Vol. 1068. pp 135-139, 2008. *In*: Advances in GaN, GaAs, SiC and Related Alloys on Silicon Substrates, Eds: Tingkai Li, Joan M. Redwing, Michael Mastro, Edwin L. Piner and Armin Dargar. © 2008 Materials Research Society (1068-C02-13).

D. Conference Abstracts

1. Yuen-Yee Wong, Edward Yi Chang, Wei-Ching Huang, Hai-Dang Trinh, Chun-Yen Chang, ***Reduction of Parallel Conduction at the Regrowth Interface of GaN Template Using Nitridation***. 38th International Symposium on Compound Semiconductors – ISCS 2011. May 22-26, 2011, Berlin, Germany.

2. T. T. Luong, Yuen-Yee Wong, Edward Yi Chang, W. C. Huang, K. L. Lin, B. T. Tran and Y. L. Hsiao, ***Improvement of AlGaN/GaN High Electron Mobility Transistor Performance by using High Temperature AlN Interlayer and Buffer Layer Grown by MOCVD***, 38th International Symposium on Compound Semiconductors – ISCS 2011. May 22-26, 2011, Berlin, Germany.

3. Wei-Ching Huang, Edward-Yi Chang, Yuen-Yee Wong, Kung-Liang Lin, Yu-Lin Hsiao, ***The Effect of Growth Parameters on InAlN/GaN Material Grown By Metal-Organic Chemical Vapor Deposition***, 38th International Symposium on Compound Semiconductors – ISCS 2011. May 22-26, 2011, Berlin, Germany.

4. H. Q. Nguyen, E. Y. Chang, H. D Trinh, H. W. Wu, Y. Y. Wong, H. H. Vu, T. B. Tran, K. L. Lin, C. C. Chung, C. H. Hsu, W. C. Wang and C. L. Nguyen, ***High Quality 1 eV InGaAs on GaAs substrate for inverted metamorphic solar cell by MOCVD***, 38th International

Symposium on Compound Semiconductors – ISCS 2011. May 22-26, 2011, Berlin, Germany.

5. H. D. Trinh, E.Y. Chang, C. I. Kuo, H. Q. Nguyen, K. L. Lin, Y. Y. Wong, C. C. Chung, Y. C. Lin, C. H. Chang, Y. S. Chiu, B. T. Tran and C. L. Nguyen, ***Atomic layer deposition of $Al_2O_3/n\text{-}In_xGa_{1-x}As$ structures with different In content ($x = 0.53\text{-}1$)***, 38th International Symposium on Compound Semiconductors – ISCS 2011. May 22-26, 2011, Berlin, Germany.

6. Yuen-Yee Wong, Edward Yi Chang, Wei-Jin Huang and Hai-Dang Trinh. ***Suppression of Parallel Conduction at the Regrowth Interface of GaN Template Using Nitrogen Plasma Treatment***. Annual meeting of the Physical Society of ROC, January 25-27, 2011, Taipei, Taiwan

7. Yuen-Yee Wong, Edward Yi Chang, Tsung-Hsi Yang, Jet-Rung Chang, Jui-Tai Ku and Kung-Liang Lin. ***Recovering of rough GaN surface grown under Ga-lean condition by plasma-assisted molecular beam epitaxy using migration enhanced epitaxy method***. Annual meeting of the Physical Society of ROC, February 2-4, 2010, Tainan, Taiwan

8. Kung-Liang Lin, Tien-Tung Luong, Chen-Hao Chiang , Yuen-Yee Wong, Yu-Lin Hsiao, Wei-Ching Huang, Jung-Chi Lu, Binh-Tinh Tran and Edward-Yi Chang. ***Electrical and Optical Characterization of GaN film grown on patterned Si (111) substrates.*** Annual meeting of the Physical Society of ROC, February 2-4, 2010, Tainan, Taiwan.

9. Hai-Dang Trinh, Edward Yi Chang, Yuen-Yee Wong, Chia-Yuan Chang, Chih-Chieh Yu, ***Electrical Characteristics of Atomic Layer Deposition Al_2O_3 on n-InAs with various surface treatments.*** Annual meeting of the Physical Society of ROC, February 2-4, 2010, Tainan, Taiwan.

10. J. T. Ku, T. H. Yang, J. R. Chang, Y. Y. Wong, C. Y. Chen, C. Y. Chang and W. C. Chou, ***Epitaxial overgrowth of GaN nano-rods on Si(111) substrates by plasma-assisted MBE.*** Annual meeting of the Physical Society of ROC, February 2-4, 2010, Tainan, Taiwan.

11. Yuen-Yee Wong, Edward Yi Chang, Tsung-Hsi Yang, Jet-Rung Chang, Jui-Tai Ku and Yi-Cheng Chen. ***Dislocation reduction in GaN film using Ga-lean GaN buffer grown by plasma-assisted molecular beam epitaxy with migration enhanced epitaxy method.*** The 8th International Conference on Nitride Semiconductors, October 18-23, 2009, ICC Jeju, Korea.